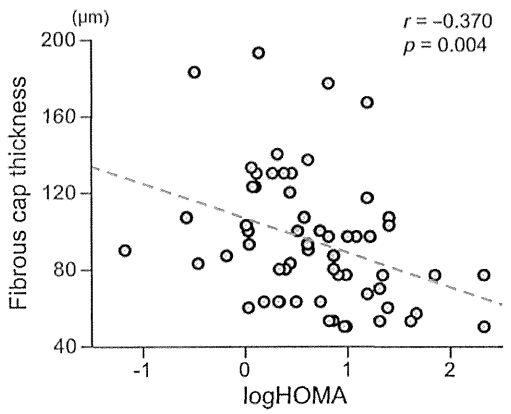

Figure 3 Correlation between log HOMA-IR and fibrous cap thickness in SAP. There was a significant correlation between log HOMA-IR and fibrous cap thickness identified by OCT in SAP ($r = -0.370$, $P = 0.004$). *r*, correlation coefficient; SAP, stable angina pectoris; other abbreviations are as in *Figure 1*.

Table 4 Logistic regression analysis for predicting the presence of TCFA

Variable	Odds ratio	95% confidence interval	*P*-value
ACS	17.98	7.12–52.02	<0.0001
DM	2.55	0.76–9.10	0.13
HOMA-IR (>2.50)	3.57	1.42–9.55	0.007
LDL-cholesterol	1.01	0.99–1.03	0.38
Statin use	0.62	0.21–1.77	0.37
Triglyceride	1.01	0.99–1.01	0.20
Hs-C-reactive protein	0.95	0.69–1.35	0.75

Adjusted for risk factors (age, sex, BMI, HT, smoking, and HbA1c level).
ACS, acute coronary syndrome; DM, diabetes mellitus; TCFA, thin-cap fibroatheroma; HOMA-IR, homeostasis model assessment of insulin resistance; LDL, low-density lipoprotein; Hs-C-reactive protein, high-sensitivity C-reactive protein.

might not be a major marker of plaque vulnerability. Since the first report of plaque rupture in 1844,[17] many clinical investigators have noted vulnerable/unstable plaque features, which lead to ACS *in vivo*. As a widely recognized histological concept, a vulnerable plaque is characterized by the presence of TCFA, and defined as a large necrotic core with a thin fibrous cap (<65 μm) and increased macrophage infiltration.[18] Currently, OCT is the best validated imaging modality for detecting vulnerable plaques, including TCFA and ruptured plaques. A recently published study demonstrated that insulin resistance calculated by HOMA-IR is an independent predictor of post-procedural myocardial injury and cardiovascular events after PCI with a drug-eluting stent.[19] Another study revealed that the presence of OCT-defined TCFA predicts post-procedural MI in PCI patients.[20] Our present study might suggest complementary relationships among insulin resistance, vulnerable plaque, and cardiovascular events after PCI. In addition, our present study demonstrated that insulin resistance was significantly associated with the presence of microvessel as identified by OCT. Intraplaque microvessels play a pivotal role in coronary plaque growth by increasing red blood cells, thereby supplying inflammatory cells and cytokines into the plaque. Sluimer *et al.*[21] revealed that microvessel was increased in advanced plaques compared with early plaques, and the microvessel mural cell coverage was incomplete in normal and atherosclerotic arteries in a human histological study. They suggested that the compromised structural integrity of intraplaque angiogenesis might explain the microvascular leakage responsible for extensive leucocyte infiltration, intraplaque haemorrhage, and plaque instability. Furthermore, a recent clinical study described that TCFA and microvessels identified by OCT were the potential predictors of subsequent progression of coronary plaques.[22] These results support our hypothesis about insulin resistance and plaque instability. To the best of our knowledge, this is the first report to evaluate the association between insulin resistance and coronary plaque components assessed by OCT.

Although the concept that systemic/local inflammation accelerates the progression of atherosclerotic plaque has been well established in a large number of previous studies,[23,24] the relationships among insulin resistance, inflammation, and plaque instability are intricately intertwined pathophysiologically. Elevated levels of pro-inflammatory cytokines such as tumour necrosis factor α, interleukin (IL)-6, IL-1β, and monocyte chemoattractant protein-1 have been shown in individuals with insulin resistance and DM.[25–27] These cytokines play important roles in the activation of macrophage foam cells, resulting in early plaque development and fibrous cap weakening. Our results demonstrated that macrophage infiltration as assessed by OCT tended to be more frequently present in the higher HOMA-IR tertile. However, our present results could not demonstrate a significant association between insulin resistance and hs-C-reactive protein level—a clinical biomarker of inflammation. C-reactive protein levels correlate well with known risk factors such as smoking, low levels of HDL-cholesterol, and obesity.[28] In addition, although we excluded the subjects with active inflammatory conditions from the present study, C-reactive protein—an acute-phase reactant produced by the liver upon stimulation by IL-6—is a non-specific indicator of inflammation and thus may not directly influence atherogenesis.[29]

Although DM is a well-known risk factor for the development of cardiovascular events, the previous studies using OCT imaging reported conflicting results as to whether continuous hyperglycaemia was associated with coronary plaque vulnerability.[5,30,31] In the present study, both the presence of DM and HbA1c level were not significantly associated with TCFA. There are potential reasons for these results. We excluded diabetic patients receiving insulin therapy who have a higher risk of in-stent restenosis and cardiovascular events than those who were treated with oral glycerides,[32] because it is difficult to assess insulin resistance in subjects receiving insulin therapy. In addition, we excluded subjects with fasting plasma glucose level >140 mg/dL from this study. There is general consensus that HOMA model is incredible when fasting glucose level is >140 mg/dL, because basal fasting insulin production becomes less responsive to increasing glucose production of >140–160 mg/dL.[33] Indeed, it has been reported that HOMA-IR showed lower

correlation with *M*-value, insulin sensitivity as the average rate of exogenous glucose infusion for 30 min, by using the euglycaemic hyperinsulinaemic clamp technique in type 2 diabetic patients with moderate hyperglycaemia (fasting plasma glucose >140 mg/dL).[34] Although we adopted strict inclusion criteria in the present study for reliable assessment of insulin resistance, we speculate these factors might attenuate the influence of DM itself for plaque instability. Furthermore, the prognostic value of HbA1c, which is an indicator of the average blood glucose concentrations over the preceding 2–3 months, in CAD remains controversial.[35,36]

The present study revealed a significant association between insulin resistance and coronary plaque vulnerability. Additional treatment with insulin sensitizer may be a suitable approach for preventing future cardiovascular events.

Study limitations

This study has several limitations. First, this study included patients with both SAP and ACS. As shown in this study, although the presence of ACS is the strongest confounding factor related to vulnerable plaques, there were no differences in the percentage of ACS among the three groups. Furthermore, multivariate analysis including ACS revealed that higher HOMA-IR values were independently related to the presence of TCFA. Second, we assessed the plaque component using both M2 and C7 OCT systems in this study. Although the use percentage of the C7 system did not significantly differ among the three groups, potential differences in the ability to detect tissue characteristics, including lipid content, TCFA, and microvessels (due to difference of frame spacing between M2 and C7), might have affected the plaque classification of the three groups. Third, intracoronary thrombi were observed in many cases with ACS. Although we excluded lesions with a large quantity of thrombi from the OCT analysis and we performed aspiration thrombectomy for lesions with delayed coronary flow, these thrombi might have affected analysis of the plaque left behind. Fourth, as we described above, the true effect of DM against plaque vulnerability cannot be properly assessed using the present study design and population (including only mild or wellcontrolled DM). Finally, this study was conducted at a single centre with a relatively small sample size. Further large-scale studies are warranted to determine whether insulin resistance as defined by HOMA-IR may predict coronary plaque progression.

Conclusions

This study demonstrated that insulin resistance assessed by HOMA-IR is independently related to coronary plaque vulnerability identified by OCT. Insulin resistance assessed by HOMA-IR might be a useful marker for risk stratification in patients with CAD.

Conflict of interest: None declared.

Funding

No authors have support or sponsors.

References

1. Haffner SM, Lehto S, Ronnemaa T, Pyorala K, Laakso M. Mortality from coronary heart disease in subjects with type 2 diabetes and in nondiabetic subjects with and without prior myocardial infarction. *N Engl J Med* 1998;**339**:229–34.
2. Norhammar A, Malmberg K, Diderholm E, Lagerqvist B, Lindahl B, Ryden L *et al.* Diabetes mellitus: the major risk factor in unstable coronary artery disease even after consideration of the extent of coronary artery disease and benefits of revascularization. *J Am Coll Cardiol* 2004;**43**:585–91.
3. Otter W, Kleybrink S, Doering W, Standl E, Schnell O. Hospital outcome of acute myocardial infarction in patients with and without diabetes mellitus. *Diabet Med* 2004;**21**:183–7.
4. Burke AP, Kolodgie FD, Zieske A, Fowler DR, Weber DK, Varghese PJ *et al.* Morphologic findings of coronary atherosclerotic plaques in diabetics: a postmortem study. *Arterioscler Thromb Vasc Biol* 2004;**24**:1266–71.
5. Kato K, Yonetsu T, Kim SJ, Xing L, Lee H, McNulty I *et al.* Comparison of nonculprit coronary plaque characteristics between patients with and without diabetes: a 3-vessel optical coherence tomography study. *JACC Cardiovasc Interv* 2012;**5**:1150–8.
6. Moreno PR, Murcia AM, Palacios IF, Leon MN, Bernardi VH, Fuster V *et al.* Coronary composition and macrophage infiltration in atherectomy specimens from patients with diabetes mellitus. *Circulation* 2000;**102**:2180–4.
7. Nasu K, Tsuchikane E, Katoh O, Fujita H, Surmely JF, Ehara M *et al.* Plaque characterisation by virtual histology intravascular ultrasound analysis in patients with type 2 diabetes. *Heart* 2008;**94**:429–33.
8. Breen DM, Giacca A. Effects of insulin on the vasculature. *Curr Vasc Pharmacol* 2011;**9**:321–32.
9. Despres JP, Lamarche B, Mauriege P, Cantin B, Dagenais GR, Moorjani S *et al.* Hyperinsulinemia as an independent risk factor for ischemic heart disease. *N Engl J Med* 1996;**334**:952–7.
10. Hanley AJ, Williams K, Stern MP, Haffner SM. Homeostasis model assessment of insulin resistance in relation to the incidence of cardiovascular disease: the San Antonio Heart Study. *Diabetes Care* 2002;**25**:1177–84.
11. An X, Yu D, Zhang R, Zhu J, Du R, Shi Y *et al.* Insulin resistance predicts progression of de novo atherosclerotic plaques in patients with coronary heart disease: a one-year follow-up study. *Cardiovasc Diabetol* 2012;**11**:71.
12. Amano T, Matsubara T, Uetani T, Nanki M, Marui N, Kato M *et al.* Abnormal glucose regulation is associated with lipid-rich coronary plaque: relationship to insulin resistance. *JACC Cardiovasc Imaging* 2008;**1**:39–45.
13. Mitsuhashi T, Hibi K, Kosuge M, Morita S, Komura N, Kusama I *et al.* Relation between hyperinsulinemia and nonculprit plaque characteristics in nondiabetic patients with acute coronary syndromes. *JACC Cardiovasc Imaging* 2011;**4**:392–401.
14. Matthews DR, Hosker JP, Rudenski AS, Naylor BA, Treacher DF, Turner RC. Homeostasis model assessment: insulin resistance and beta-cell function from fasting plasma glucose and insulin concentrations in man. *Diabetologia* 1985;**28**:412–9.
15. Reiber JH, Serruys PW, Kooijman CJ, Wijns W, Slager CJ, Gerbrands JJ *et al.* Assessment of short-, medium-, and long-term variations in arterial dimensions from computer-assisted quantitation of coronary cineangiograms. *Circulation* 1985;**71**:280–8.
16. Prati F, Regar E, Mintz GS, Arbustini E, Di Mario C, Jang IK *et al.* Expert review document on methodology, terminology, and clinical applications of optical coherence tomography: physical principles, methodology of image acquisition, and clinical application for assessment of coronary arteries and atherosclerosis. *Eur Heart J* 2010;**31**:401–15.
17. Herrick JB. Landmark article (JAMA 1912). Clinical features of sudden obstruction of the coronary arteries. By James B. Herrick. *JAMA* 1983;**250**:1757–65.
18. Virmani R, Kolodgie FD, Burke AP, Farb A, Schwartz SM. Lessons from sudden coronary death: a comprehensive morphological classification scheme for atherosclerotic lesions. *Arterioscler Thromb Vasc Biol* 2000;**20**:1262–75.
19. Uetani T, Amano T, Harada K, Kitagawa K, Kunimura A, Shimbo Y *et al.* Impact of insulin resistance on post-procedural myocardial injury and clinical outcomes in patients who underwent elective coronary interventions with drug-eluting stents. *JACC Cardiovasc Interv* 2012;**5**:1159–67.
20. Lee T, Yonetsu T, Koura K, Hishikari K, Murai T, Iwai T *et al.* Impact of coronary plaque morphology assessed by optical coherence tomography on cardiac troponin elevation in patients with elective stent implantation. *Circ Cardiovasc Interv* 2011;**4**:378–86.
21. Sluimer JC, Kolodgie FD, Bijnens AP, Maxfield K, Pacheco E, Kutys B *et al.* Thin-walled microvessels in human coronary atherosclerotic plaques show incomplete endothelial junctions relevance of compromised structural integrity for intraplaque microvascular leakage. *J Am Coll Cardiol* 2009;**53**:1517–27.
22. Uemura S, Ishigami K, Soeda T, Okayama S, Sung JH, Nakagawa H *et al.* Thin-cap fibroatheroma and microchannel findings in optical coherence tomography correlate with subsequent progression of coronary atheromatous plaques. *Eur Heart J* 2012;**33**:78–85.
23. Carter AM. Inflammation, thrombosis and acute coronary syndromes. *Diab Vasc Dis Res* 2005;**2**:113–21.
24. Ikeda U. Inflammation and coronary artery disease. *Curr Vasc Pharmacol* 2003;**1**:65–70.
25. Mita T, Goto H, Azuma K, Jin WL, Nomiyama T, Fujitani Y *et al.* Impact of insulin resistance on enhanced monocyte adhesion to endothelial cells and atherosclerogenesis independent of LDL cholesterol level. *Biochem Biophys Res Commun* 2010;**395**:477–83.
26. Olefsky JM, Glass CK. Macrophages, inflammation, and insulin resistance. *Annu Rev Physiol* 2010;**72**:219–46.

27. Deepa R, Velmurugan K, Arvind K, Sivaram P, Sientay C, Uday S *et al.* Serum levels of interleukin 6, C-reactive protein, vascular cell adhesion molecule 1, and monocyte chemotactic protein 1 in relation to insulin resistance and glucose intolerance—the Chennai Urban Rural Epidemiology Study (CURES). *Metabolism* 2006;**55**:1232–8.
28. Miller M, Zhan M, Havas S. High attributable risk of elevated C-reactive protein level to conventional coronary heart disease risk factors: the Third National Health and Nutrition Examination Survey. *Arch Intern Med* 2005;**165**:2063–8.
29. Scirica BM, Morrow DA. Is C-reactive protein an innocent bystander or proatherogenic culprit? The verdict is still out. *Circulation* 2006;**113**:2128–34; Discussion 2151.
30. Chia S, Raffel OC, Takano M, Tearney GJ, Bouma BE, Jang IK. Comparison of coronary plaque characteristics between diabetic and non-diabetic subjects: an in vivo optical coherence tomography study. *Diabetes Res Clin Pract* 2008;**81**:155–60.
31. Feng T, Yundai C, Lian C, Zhijun S, Changfu L, Jun G *et al.* Assessment of coronary plaque characteristics by optical coherence tomography in patients with diabetes mellitus complicated with unstable angina pectoris. *Atherosclerosis* 2010;**213**:482–5.
32. Kumar R, Lee TT, Jeremias A, Ruisi CP, Sylvia B, Magallon J *et al.* Comparison of outcomes using sirolimus-eluting stenting in diabetic versus nondiabetic patients with comparison of insulin versus non-insulin therapy in the diabetic patients. *Am J Cardiol* 2007;**100**:1187–91.
33. DeFronzo RA, Ferrannini E, Simonson DC. Fasting hyperglycemia in non-insulin-dependent diabetes mellitus: contributions of excessive hepatic glucose production and impaired tissue glucose uptake. *Metabolism* 1989;**38**:387–95.
34. Matsuhisa M, Yamasaki Y, Emoto M, Shimabukuro M, Ueda S, Funahashi T *et al.* A novel index of insulin resistance determined from the homeostasis model assessment index and adiponectin levels in Japanese subjects. *Diabetes Res Clin Pract* 2007;**77**:151–4.
35. Gerstein HC, Miller ME, Byington RP, Goff DC Jr, Bigger JT, Buse JB *et al.* Effects of intensive glucose lowering in type 2 diabetes. *N Engl J Med* 2008;**358**:2545–59.
36. Liu Y, Yang YM, Zhu J, Tan HQ, Liang Y, Li JD. Prognostic significance of hemoglobin A1c level in patients hospitalized with coronary artery disease. A systematic review and meta-analysis. *Cardiovasc Diabetol* 2011;**10**:98.

IMAGE FOCUS

doi:10.1093/ehjci/jet179
Online publish-ahead-of-print 10 October 2013

Visualization of pericarditis by fluorodeoxyglucose PET

Soile Pauliina Salomäki[1]*, Ulla Hohenthal[1], Jukka Kemppainen[2,3], Laura Pirilä[1], and Antti Saraste[2,4]

[1]Division of Medicine, Turku University Hospital, Turku, Finland; [2]Turku PET Centre, University of Turku, Turku, Finland; [3]Department of Clinical Physiology and Nuclear Medicine, Turku University Hospital, Turku, Finland; and [4]Heart Centre, Turku University Hospital and University of Turku, Turku, Finland

* Corresponding author. Tel: + 358 503031389; fax: +358 23132030. Email: soile.salomaki@utu.fi

We describe a case of postpericardiotomy syndrome imaged by positron emission tomography (PET) with ^{18}F-fluorodeoxyglucose (^{18}F-FDG) and computed tomography (CT).

A 53-year-old woman had surgical aortic valve replacement with mechanical prosthesis due to severe aortic valve regurgitation. Within 1 month of surgery, she was diagnosed inflammatory pericarditis with 2 cm of excess pericardial fluid by echocardiography (Panel *D*, pericardial space between arrows). The postpericardiotomy syndrome responded well to colchicine treatment.

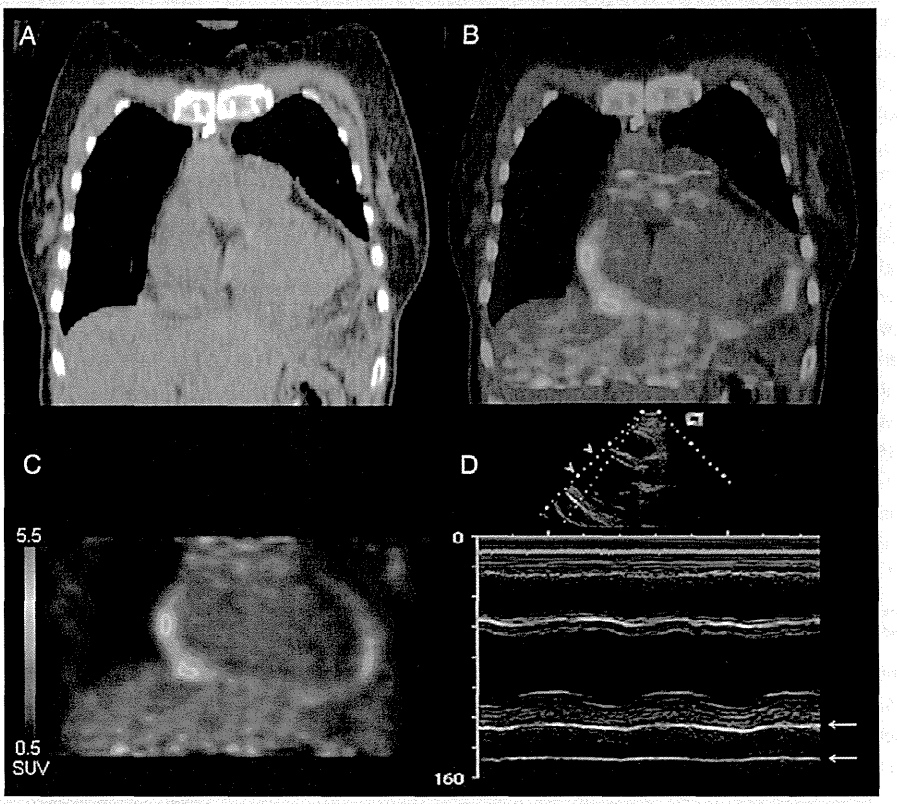

Two months after the operation she was re-admitted to the hospital because of fever, raised C-reactive protein level (275 mg/L) and leukocytosis. Blood cultures were negative and the procalcitonin level was normal (0.18 μg/L). Transoesophageal echocardiography showed normal function of the aortic valve prosthesis and no vegetations or other signs of endocarditis. There was only a small amount of pericardial fluid (up to 4 mm).

To detect focus of infection, PET and CT with ^{18}F-FDG was performed. Physiological FDG uptake in the myocardium was efficiently suppressed by patient preparation with non-carbohydrate diet and overnight fast. However, there was strong metabolic activity surrounding the heart co-localizing with the pericardium (*Panels A–C*). Maximum standardized uptake value was 5.0. There was mild ^{18}F-FDG uptake associated with the aortic valve prosthesis and few reactive lymph nodes in the thoracic area.

The ^{18}F-FDG PET/CT revealed active postpericardiotomy syndrome. Treatment was continued with colchicine and corticosteroids, without antibiotics. Inflammatory markers and clinical condition normalized quickly.

To our knowledge, this is the first case showing pericardial inflammation by ^{18}F-FDG PET/CT.

Biochemical and Biophysical Research Communications 445 (2014) 327–333

Contents lists available at ScienceDirect

Biochemical and Biophysical Research Communications

journal homepage: www.elsevier.com/locate/ybbrc

Lipid synthesis is promoted by hypoxic adipocyte-derived exosomes in 3T3-L1 cells

Soichi Sano [a], Yasukatsu Izumi [a,b,*], Takehiro Yamaguchi [a], Takanori Yamazaki [a], Masako Tanaka [b], Masayuki Shiota [b], Mayuko Osada-Oka [c], Yasuhiro Nakamura [d], Min Wei [e], Hideki Wanibuchi [e], Hiroshi Iwao [b], Minoru Yoshiyama [a]

[a] Department of Cardiovascular Medicine, Osaka City University Graduate School of Medicine, Osaka, Japan
[b] Department of Pharmacology, Osaka City University Graduate School of Medicine, Osaka, Japan
[c] Food Hygiene and Environmental Health, Kyoto Prefectural University, Graduate School of Life and Environmental Sciences, Kyoto, Japan
[d] Department of Cardiology, Izumi Municipal Hospital, Izumi-Osaka, Japan
[e] Department of Pathology, Osaka City University Graduate School of Medicine, Osaka, Japan

ARTICLE INFO

Article history:
Received 27 January 2014
Available online 7 February 2014

Keywords:
Adipocytes
Exosome
Hypoxia
Proteomic analysis
De novo lipogenesis

ABSTRACT

Hypoxia occurs within adipose tissues as a result of adipocyte hypertrophy and is associated with adipocyte dysfunction in obesity. Here, we examined whether hypoxia affects the characteristics of adipocyte-derived exosomes. Exosomes are nanovesicles secreted from most cell types as an information carrier between donor and recipient cells, containing a variety of proteins as well as genetic materials. Cultured differentiated 3T3-L1 adipocytes were exposed to hypoxic conditions and the protein content of the exosomes produced from these cells was compared by quantitative proteomic analysis. A total of 231 proteins were identified in the adipocyte-derived exosomes. Some of these proteins showed altered expression levels under hypoxic conditions. These results were confirmed by immunoblot analysis. Especially, hypoxic adipocyte-released exosomes were enriched in enzymes related to *de novo* lipogenesis such as acetyl-CoA carboxylase, glucose-6-phosphate dehydrogenase, and fatty acid synthase (FASN). The total amount of proteins secreted from exosomes increased by 3–4-fold under hypoxic conditions. Moreover, hypoxia-derived exosomes promoted lipid accumulation in recipient 3T3-L1 adipocytes, compared with those produced under normoxic conditions. FASN levels were increased in undifferentiated 3T3-L1 cells treated with FASN-containing hypoxic adipocytes-derived exosomes. This is a study to characterize the proteomic profiles of adipocyte-derived exosomes. Exosomal proteins derived from hypoxic adipocytes may affect lipogenic activity in neighboring preadipocytes and adipocytes.

1. Introduction

Adipose tissues store excess energy in the form of lipids [1,2]. The tissues are the largest energy reserve in mammals and are capable of accommodating prolonged nutrient excess by altering their mass. However, abnormal or excess accumulation of lipids in adipose tissues causes obesity, which may impair health [3–5]. Adipose tissue expansion occurs when adipocyte numbers and size increase, which is known as hyperplasia and hypertrophy, respectively [6]. Limiting adipocyte hyperplasia leads to lipid accumulation in existing adipocytes, resulting in hypertrophy. Uptake of exogenous lipids or synthesis of endogenous lipids in the cytosol causes hypertrophy. Smaller adipocytes may be more likely to synthesize fatty acids endogenously (*de novo* lipogenesis) to begin the lipids accumulation process, while uptake of exogenous fatty acids is more predominant in developing cells [7].

De novo lipogenesis [8] is the process in which non-lipid precursors are converted to fatty acids, and requires acetyl-CoA, which is generated during various metabolic processes. Acetyl-CoA provides the carbon atoms necessary for fatty acid synthesis. It is converted to malonyl-CoA, and the rate-limiting steps in *de novo* lipogenesis are catalyzed mainly by acetyl-CoA carboxylase (ACC). Successive

Abbreviations: ACN, acetonitrile; ACC, acetyl-CoA carboxylase; FASN, fatty acid synthase; FBS, fetal bovine serum; G6PD, glucose-6-phosphate dehydrogenase; GAPDH, glyceraldehyde-phosphate dehydrogenase; Hsc70, heat shock cognate 71 kDa protein; Hsp, heat shock protein; Hsp72, heat shock 71 kDa protein 1A; HIF-1α, hypoxia-inducible factor-1α; WT, wild-type.

* Corresponding author at: Department of Pharmacology, Osaka City University Graduate School of Medicine, 1-4-3 Asahi-machi, Abeno-ku, Osaka 545-8585, Japan.
E-mail address: izumi@msic.med.osaka-cu.ac.jp (Y. Izumi).

http://dx.doi.org/10.1016/j.bbrc.2014.01.183
0006-291X/

malonyl-CoA molecules, which serve as a two-carbon donor, are added to acetyl-CoA by the multi-functional enzyme complex, fatty acid synthase (FASN). Glucose-6-phosphate dehydrogenase (G6PD) is a key enzyme that supplies the cellular NADPH required for lipid biosynthesis.

Adipocytes have a limited capacity to accumulate lipid droplets. When adipocytes suffer from lipid overload, hypoxia develops; the reduction in oxygen tension is directly linked to adipocyte dysfunction. To avoid lipid overload and the associated cellular stress in adipose tissues, expression of enzymes related to *de novo* lipogenesis is reduced [9]. Additionally, adipocytes do not increase in size in a synchronized fashion [10]. Small adipocytes and preadipocytes can act as reservoirs by increasing their storage capacity when larger adipocytes no longer accommodate increased lipid storage. However, how adipocytes without lipid overload are activated to store excess energy remains unknown. Adipocytes communicate with each other and with other tissues [11], but the types of communication between stressed larger adipocytes under hypoxic stress and non-stressed, less hypoxic adipocytes are unknown. Three types of signals are known to control communication between adipocytes [11]: cell-to-cell contact, soluble factors, and exosomes.

Exosomes are small 50–150 μm membrane vesicles secreted from most cell types [12]; they play an important role as information carriers between donor and recipient cells. Exosomes contain a wide variety of cytosolic contents as well as membranous components from donor cells, including genetic materials, lipids, and proteins, which determine the types of information carried [13,14]. Exosome content is thought to reflect the conditions surrounding the donor cells [15]. Exosomes could fuse with and transfer their internal contents into the cytosol of recipient cells [14]. Upon interacting with exosomes and receiving the internal contents, recipient cells undergo morphological and physiological changes, including cancer metastasis, angiogenesis, and cell differentiation [16–19]. Adipocytes also secrete exosomes [20]; however, the characteristics of adipocyte-derived exosomes are poorly understood, particularly under pathological conditions.

In this study, we first conducted quantitative proteomic analysis in 3T3-L1 adipocyte-derived exosomes. We demonstrated that multiple enzymes related to *de novo* lipogenesis were enriched in exosomes secreted under hypoxic conditions. These exosomes may promote lipid accumulation by transferring lipogenic enzymes into recipient cells.

2. Materials and methods

2.1. Reagents, cell lines, and animals

Detailed material information can be found in the data supplement.

2.2. Exosome purification

Donor cells (3T3-L1 cells or HEK 293T cells) were cultured in DMEM (4500 mg/L glucose) supplemented with 10% exosomes-depleted fetal bovine serum (FBS). Exosomes were depleted of FBS by 12 h ultracentrifugation at 100,000*g*, 4 °C. Exosomes were prepared from cell supernatants using sequential centrifugation and filtration steps. Briefly, cell supernatants were diluted in an equal volume of phosphate-buffered saline (PBS) and centrifuged for 30 min at 2000*g*, 4 °C. The supernatants were centrifuged for 60 min at 10,000*g*, 4 °C. Next, the supernatants were ultracentrifuged for 3 h at 100,000*g*, 4 °C. Pellets were resuspended in a large volume of PBS and the suspension was filtered through a 0.22-μm filter. Exosomes were pelleted by 3 h of ultracentrifugation at 100,000*g*, 4 °C. Total amount of exosomes was determined by using the BCA assay (Thermo Scientific, Rockford, IL, USA). Purified exosomes were resuspended in PBS and stored at −80 °C until use.

2.3. Electron microscopy analysis

PBS-resuspended exosomes were deposited onto formvar/carbon-coated EM grids (EMJapan Co., Ltd., Tokyo, Japan). Membranes were allowed to absorb for 10 min in a dry environment; excess liquid was removed gently using absorbent paper. Exosome-coated grids were stained with 1% uranyl acetate and the preparations were examined under a transmission electron microscope (TEM; H-7500, JEOL Ltd., Tokyo, Japan).

2.4. Proteomic analysis of purified exosomes

Exosomes purified from supernatants of 3T3-L1 adipocytes under normoxic (20% O_2) or hypoxic (1% O_2) for 48 h were solubilized in 0.8% RapiGest SF (Waters, Milford, MA, USA) and lysed by 3 freeze–thaw cycles in liquid nitrogen under sonication. Next, 60 μg of exosomal proteins were reduced, alkylated, digested with trypsin, and labeled with 2-plex iTRAQ reagents (AB Sciex, Framingham, MA, USA) according to the manufacturer's instructions with minor modifications. After the labeling reaction (114, Normoxia; 116, hypoxia), the 2 samples were pooled and 10 μL of 20% (v/v) trifluoroacetic acid was added to cleave the RapiGest. Samples were vortexed, incubated at 37 °C for 1 h and centrifuged. Supernatants were purified using a cation exchange column (AB Sciex) using standard procedures, as previously described [21]. Briefly, mobile phase A contained 98% water (2% acetonitrile (ACN), 0.1% formic acid) and mobile phase B contained 70% ACN (0.1% formic acid, 30% water). The column effluent was introduced into a spray chamber through a tapered stainless steel emitter and directly electrosprayed into the QSTAR System ion trap mass spectrometer in positive mode for nanoESI-tandem mass spectrometry (MS/MS) analysis. Each sample was run for 150 min. Protein identification was performed using Analyst QS Software 2.0 (AB Sciex) in positive-ion mode. Both data sets were processed using ProteinPilot Software 2.0.1 with the Paragon™ search algorithm (AB Sciex). MS/MS data were searched against the NCBI database using a *Mus musculus* taxonomy filter. The minimum threshold for protein identification was set at a protein score of 0.47, corresponding to a confidence level >66% and 1% false discovery rate.

2.5. Immunoblot analysis

Detailed material information can be found in the data supplement.

2.6. Exosomes taken up by 3T3-L1 cells

For red fluorescent labeling of cells, we incubated HEK 293T cells with PKH26 (Sigma–Aldrich, St. Louis, MO, USA) according to the manufacturer's instructions. 3T3-L1 preadipocytes were cultured in media containing PKH26 exosomes.

2.7. Statistical analysis

All data are presented as means ± SD. Data were analyzed using paired Student's *t*-test. $P < 0.05$ was considered significant.

3. Results

3.1. Serum exosomes are increased in obese animals

To examine whether obesity affects serum exosomes, serum exosomes from leptin-deficient (ob/ob) obesity mice and wild-type

(WT) mice were isolated. Exosomes from ob/ob mouse serum contained more protein amount than WT mouse serum (Fig. 1A). Notably, the amount of exosomal protein in ob/ob mice was similar to that in WT mice after compensating for body weight (Fig. 1B), indicating that the increase of serum exosomes in ob/ob mice was due to increased body weight.

3.2. Hypoxia enhances exosome secretion in 3T3-L1 adipocytes

Next, using 3T3-L1 cells as a model of differentiated-adipocytes, we examined whether adipocytes secrete exsomes. Conditioned medium were collected from pre-differentiated or differentiated 3T3-L1 cells after 24–48 h culture under normoxic conditions. Sequential centrifugation steps with increasing centrifugal forces up to 100,000*g* yielded a greasy pellet, which contained the exosomes (Fig. 1C). TEM analysis revealed that both conditioned medium from pre-differentiated and differentiated 3T3-L1 cells contained 50–150 μm intact membrane vesicles with typical exosome morphology (Fig. 1D).

Substantial evidence indicates that hypoxia develops in adipose tissue as the tissue mass expands, contributing to adipocyte dysfunction in obese animals [22]. Therefore, we examined the effect of hypoxia on exosome secretion of 3T3-L1 adipocytes. Expression of hypoxia-inducible factor-1α (HIF-1α), a regulator of hypoxic response, was markedly up-regulated under hypoxic conditions (Fig. 1E). As in normoxic 3T3-L1 adipocytes, 3T3-L1 adipocytes under hypoxic conditions secreted exosomes (Fig. 1E). Additionaly, 3T3-L1 adipocytes under hypoxic conditions showed a 3–4-fold increase in exosome secretion based on protein levels (Fig. 1F).

3.3. Exosomes from hypoxic 3T3-L1 adipocytes contain more lipogenic enzymes

To investigate whether hypoxic stress is reflected in exosomal protein content, we performed silver staining. Interestingly, a different protein band pattern was observed in 3T3-L1 adipocyte-derived exosomes under normoxic and hypoxic conditions (Supplementary Fig. 1). Additionally, we performed iTRAQ-based quantitative proteomic analysis. 3T3-L1 adipocyte-derived exosomes purified from normoxic or hypoxic culture conditions were analyzed using liquid chromatography–MS/MS. A total of 231 proteins were identified, with measured weighted median protein ratios reported in the Supplementary Tables 1–3 (ratio of hypoxia to normoxia, 116:114). A higher than 1.2-fold increase or less than 0.8-fold decrease was considered biologically significant. Among these, 75 and 67 exosomal proteins were up-regulated and down-regulated under hypoxic conditions, respectively. (Fig. 2A, and Supplementary Table 1A–C).

To confirm the quantitative proteomics data, the differential abundance of a subset of proteins was investigated using

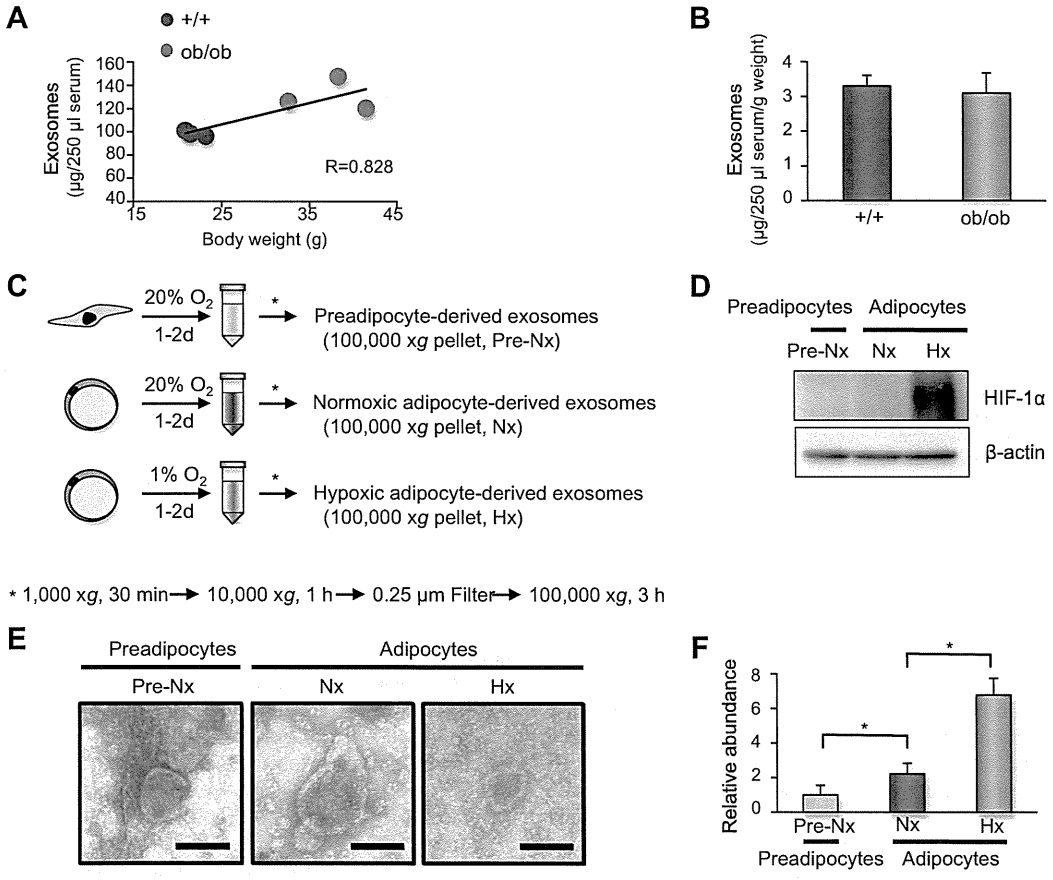

Fig. 1. Characterization of adipocyte-derived exosomes under hypoxic conditions. (A) Serum exosomes were purified from 7-week-old WT (+/+) and ob/ob mice using ExoQuick™ reagent and exosomal proteins per unit serum were determined. The graph represents the ratio of protein in serum exosomes for each group. Values are mean ± SD (each $n = 3$). *$P < 0.01$. (B) Data in (A) are corrected by body weight. Values are mean ± SD. (C) Flow chart of differential centrifugation-based protocol for exosome purification from culture supernatants. (D) Expression level of HIF-1α protein in 3T3-L1 preadipocytes and adipocytes cultured under normoxic or hypoxic conditions for 24 h. (E) Morphology of 3T3-L1 preadipocyte- and adipocyte-derived exosomes from normoxic or hypoxic conditions visualized by electron microscopy. Scale bar, 100 nm. (F) Protein concentrations in preadipocyte- and adipocyte-derived exosomes generated under normoxic or hypoxic conditions. The graph represents the ratio of normoxic exosomal proteins to hypoxic proteins. Values are mean ± SD ($n = 3$). *$P < 0.01$. 3T3-L1 adipocytes 10 days post differentiation were used for assays in (C)–(F).

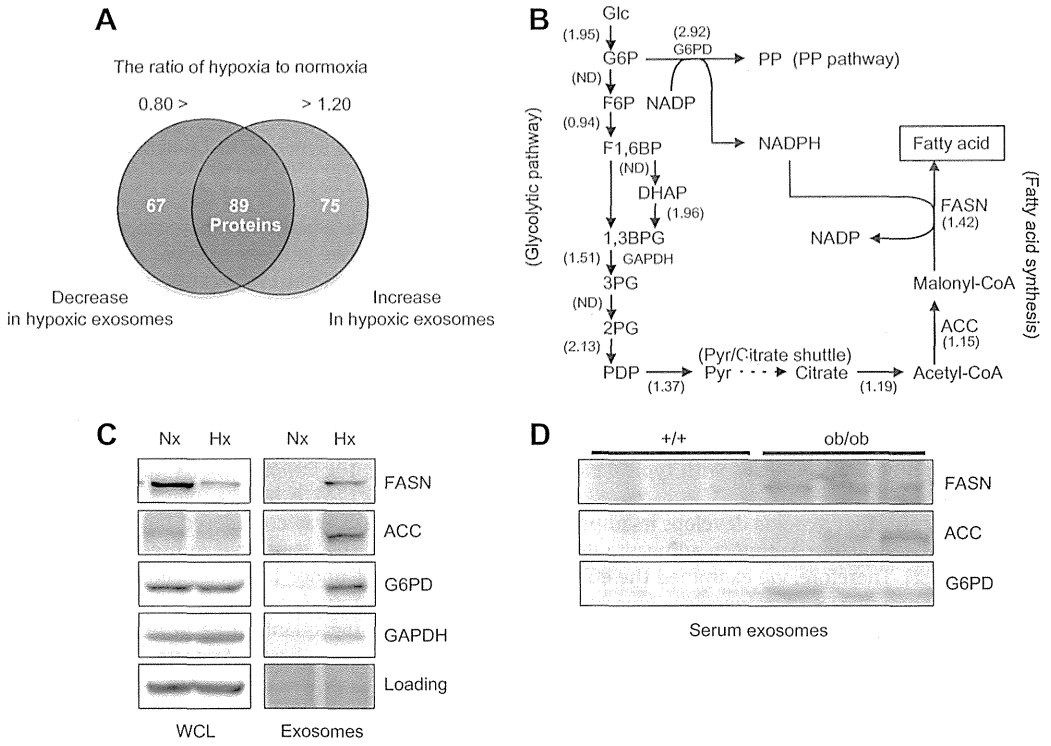

Fig. 2. Proteomic analysis of adipocyte-derived exosomes from normoxic or hypoxic conditions. (A) Comparison of proteins identified in adipocyte-derived exosomes under normoxic or hypoxic conditions. A total of 231 proteins were identified; a ratio under 0.80 was considered a decrease, while that over 1.20 was considered an increase. (B) Metabolic pathways leading to fatty acid production and its related enzymes. (C) FASN, ACC, and G6PD expression levels in whole cell lysates (WCL) and exosomes by Western blot analysis. ImmunoGold is a control blot of exosomal proteins. (D) FASN, G6PD, and GAPDH expression levels in serum exosomes from 7-week-old WT (+/+) and ob/ob mice by Western blot analysis.

Table 1
Up-regulated proteins in hypoxic adipocyte-derived exosomes, compared to control (>1.20-fold).

Accession numbers	Protein names	Unique peptdes detected	Sequencecoverage%	116:114 (Nx:Hx)	Expectation-value
gi|93102409	Fatty acid synthase	18	19	1.42	1.70E-22
gi|31981562	Pyruvate kinase isozymes M1/M2 isoform 1	6	22	1.37	1.32E-05
gi|33859482	Elongation factor 2	5	8	1.53	1.34E-05
gi|70794816	Uncharacterized protein LOC433182	5	21	1.34	3.62E-05
gi|6679937	Glyceraldehyde-3-phosphate dehydrogenase	4	21	1.51	1.91E-05
gi|6678483	Ubiquitin-like modifier-activating enzyme 1 isoform 1	4	10	1.51	2.67E-06
gi|6755901	Tubulin alpha-1A chain	4	18	1.41	5.03E-05
gi|309264022	PREDICTED: 40S ribosomal protein SA-like	3	19	1.88	2.15E-04
gi|31980648	ATP synthase subunit beta, mitochondrial precursor	3	10	1.81	1.04E-03
gi|52353955	D-3-phosphoglycerate dehydrogenase	3	8	1.68	8.92E-03

This table included up-regulated proteins having at least 3 unique peptides with ⩾99% confidence using ProteinPilot 2.0 software. Accession numbers are from the NCBI database. For additional information, see Supplementary Tables 1A and 2).

immunoblot analysis. In agreement with the proteomics data, an increase in heat shock protein (Hsp) 90 kDa -alpha, and -beta (Hsp90α, Hsp90β) and heat shock cognate 71 kDa protein (Hsc70) was found. In exosomes from 3T3-L1 adipocytes cultured under hypoxic conditions, heat shock 71 kDa protein 1A (Hsp72) was slightly decreased under hypoxic conditions, and Hsp60 was not detected, in agreement with our quantitative proteomics analysis.

From the proteomic analysis, we found that FASN was identified with significantly high confidence (Tables 1 and Supplementary Tables 1A and 2), and thereby focused on this enzyme in later analysis. Moreover, some of enzymes that could lead to fatty acids production were included among the proteins increased in hypoxic adipocyte-derived exosomes (Fig. 2B). In agreement with the proteomics data, an increase in FASN and G6PD was confirmed by immunoblot analysis. The ACC level was also increased in hypoxic adipocyte-derived exosomes, although the level was not statistically significant in proteomic analysis (Fig. 2C).

We next investigated whether such lipogenic factors were increased in serum exosomes, although serum contains both adipocyte-derived exosomes and a wide variety of tissue- and cell-derived exosomes. Serum exosomes from ob/ob mice showed increased protein levels of FASN, ACC and G6PD, compared with age- and sex-matched WT mice (Fig. 3D). Adipose tissue from WT and ob/ob mice expressed similar protein levels of FASN, ACC and G6PD (Supplementary Fig. 3).

3.4. Hypoxic adipocyte-derived exosomes promote lipogenesis

We examined whether 3T3-L1 adipocyte-derived exosomes induce changes in recipient cells, particularly regarding FASN. 3T3-L1

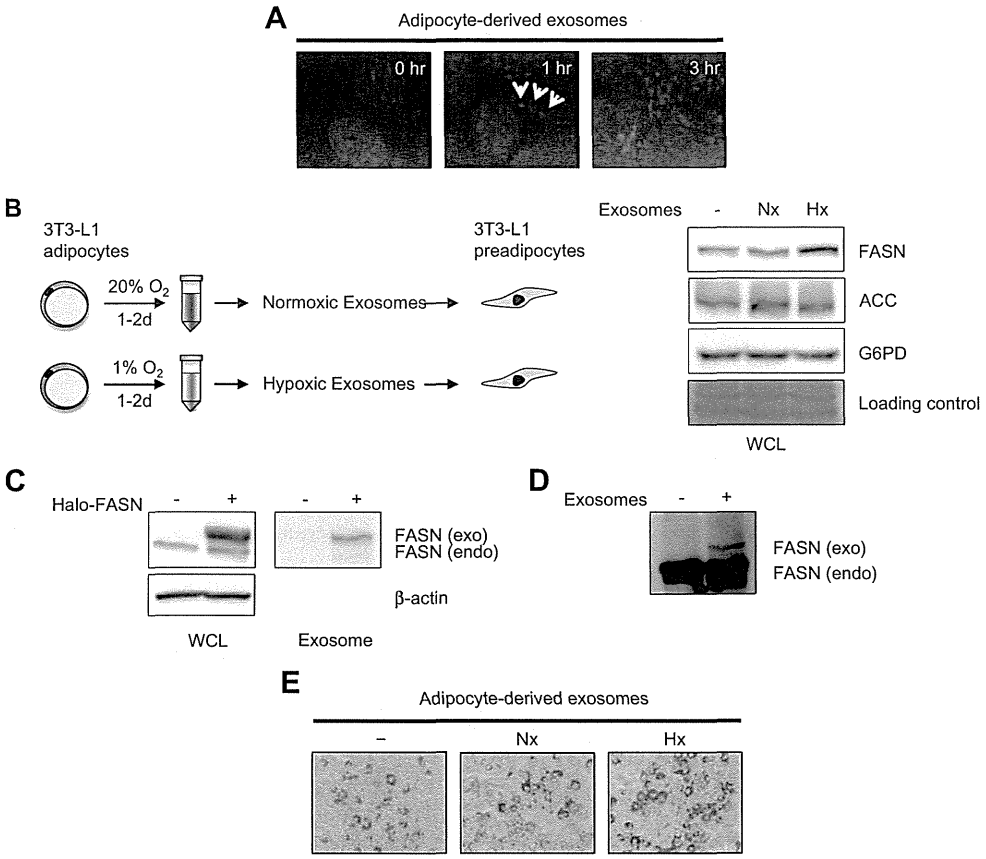

Fig. 3. Increased iipid accumulation in adipocytes treated with hypoxic adipocyte-derived exosomes. (A) Time-dependent uptake of adipocyte-derived exosomes in 3T3-L1 preadipocytes. PKH26-labeled exosomes (*red*) were added to 3T3-L1 cells and incubated as indicated. Cells were fixed and stained for nuclei (DAPI, *blue*). (B) Lysates from 3T3-L1 preadipocytes after incubation with exosomes from differentiated 3T3-L1 adipocytes cultured under normoxic or hypoxic conditions for 48 h were subjected to Western blot analysis using the indicated antibodies (FASN, ACC, and G6PD). (C) HEK 293T cells were transfected with plasmid encoding Halo-FASN. In Western blotting analysis, the same amounts of cell lysates (20 μg) and exosomes (1 μg) were loaded into the indicated lanes. (D) Lysates from 3T3-L1 preadipocytes after incubation with exosomes from HEK 293T cells transfected with plasmid encoding Halo-FASN were subjected to Western blot analysis using the anti-FASN antibody. (E) 3T3-L1 cells were induced to differentiate after confluence with a cocktail of hormones/steroids as described in the Section 2 for 6 days. 100 μg of adipocyte-derived exosomes from normoxic or hypoxic conditions was added to culture medium every 2 days. Original magnificaiton 100×.

preadipocytes were selected as recipient cells because this cell line accumulates cytosolic lipid droplets upon differentiation to adipocytes and its ease of use in assessing promoted lipogenesis.

First, we examined whether 3T3-L1 adipocyte-derived exosomes under normoxic conditions are internalized by 3T3-L1 preadipocytes. Exosomes labeled with PKH26 dye were added to 3T3-L1 preadipocytes. An efficient increase in the PKH26-derived signal from 3T3-L1 preadipocytes occurred in a time-dependent manner (Fig. 3A). Confocal microscopy confirmed that exosomes were inside 3T3-L1 preadipocytes rather than attached to the cell surface, suggesting that 3T3-L1 adipocyte-derived exosomes were taken in by 3T3-L1 preadipocytes.

We next examined whether proteins carried in exosomes can be transferred between donor and recipient cells. Recipient 3T3-L1 preadipocytes with 3T3-L1 adipocyte-derived exosomes were harvested from normoxic or hypoxic conditions. FASN level was elevated in recipient cells cultured with exosomes from hypoxic 3T3-L1 adipocytes (Fig. 3B). However, G6PD and ACC levels in recipient cells were not increased. To demonstrate that the increased FASN level was not a result of increased endogenous FASN expression but due to exosomal transfer, Halo-tagged FASN was expressed in human embryonic kidney (HEK 293T) cells, and exosomes were purified from untransfected or Halo-FASN-transfected cells. Exosomes from Halo-tagged FASN-overexpressed HEK 293T cells contained Halo-tagged FASN protein (Fig. 3c). 3T3-L1 cells incubated with purified exosomes including Halo-tagged FASN confirmed the transfer of Halo-FASN protein in exosomes into 3T3-L1 cells (Fig. 3D). These results suggest that exosomal FASN is transferred into recipient cells.

To determine whether exosomes from hypoxic 3T3-L1 adipocytes modify adipose differentiation in 3T3-L1 cells, we first examined the effect of exosomes maintained in cell culture during adipose differentiation. Normoxic exosomes did not show remarkable changes in lipid accumulation, while hypoxic exosome treatment of 3T3-L1 cells during preadipocyte differentiation enhanced lipogenesis and induced deposits of lipid droplets (Fig. 3D).

4. Discussion

Cellular stress conditions are reflected in the content of cell-derived exosomes [15]. Exosomes contain genetic materials and protein from the cell of origin, and thus depend on the stresses of the donor cells at the time of exosome biogenesis. Exosomes modulate the physiological functions of recipient cells through the transfer of RNA and proteins [14]. Exosomes exposed to some stress have been suggested to generally induce tolerance against

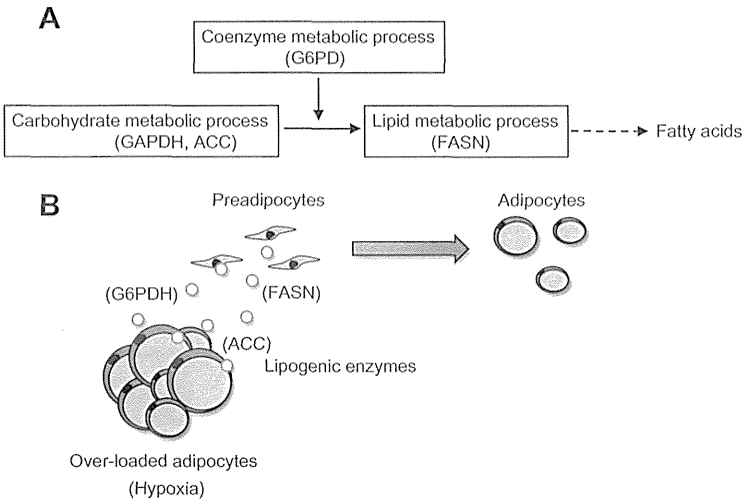

Fig. 4. Schematic representation of this study. (A) Relationship between ACC, G6PD, and FASN and *de novo* lipogenesis. (B) Promotion of lipid accumulation in preadipocytes or small adipocytes due to hypoxic adipocyte-derived exosomes.

further stresses in recipient cells [23]. Although adipocytes secrete exosomes [20], the functions of adipocyte-derived exosomes in pathological situations are poorly understood.

We here characterized the proteome profiles of mouse 3T3-L1 adipocyte-derived exosomes and evaluated the effect of hypoxia on adipocyte-derived exosomes as a stress model mimicking hypertrophied adipocytes. Lipid overload and subsequent hypertrophy of adipocytes triggers hypoxia due to insufficient blood supply [24]. We also demonstrated that both protein amounts and composition in adipocyte-derived exosomes varied significantly depending on the oxygen pressure under which cells were cultured. This suggests that adipocytes employ exosome-mediated cell communication to transfer information under hypoxic conditions. Using electron microscopy, isolated vesicles were found to have characteristisc that werre typical of exosomes [25]. Several exosome marker proteins, such as Hsp70, CD81 [26], and flotillin [27] were also detected in proteomics data. The amount of secreted exosome-associated proteins increased by 3–4-fold from adipocytes under hypoxic conditions. A recent study reported that several cell lines increase the number of exosomes under hypoxia [28], while others do not, even when exposing to hypoxia [18]. Whether increased exosome-associated proteins in hypoxic adipocytes are due to an increased number of exosomes or increased protein content in exosomes remains unknown. Using proteomic methods, we found that hypoxic adipocyte-derived exosomes showed much different protein profiles compared with normoxic exosomes. We subjected exosomal proteins to quantitative proteomics and identified 231 proteins. Seventy-five proteins were increased and 67 proteins were decreased in hypoxic 3T3-L1 adipocyte-derived exosomes. Analysis of enriched GO-terms showed that proteins related to metabolic processes were significantly increased in hypoxic adipocyte-derived exosomes. Interestingly, enzymes related to *de novo* lipogenesis such as G6PD, ACC, and FASN [8] were increased.

We found that adipocyte-derived exosomes from hypoxic conditions, which contain lipogenic enzymes, promote lipid accumulation in non-stressed, normoxic cells. Multi-enzyme complex FASN catalyzes palmitic acid synthesis from acetyl-CoA and ACC-produced malonyl-CoA in the presence of G6PD-produced NADPH (Fig. 4A). Therefore, upon exosomal transfer, donor hypoxic adipocytes may transfer the "lipogenic system", in which fatty acid synthesis is encoded, to recipient cells. As a result, donor cells decrease lipogenic enzymes, while recipient cells may increase these enzymes (Fig. 4B). Because the levels of FASN [29], G6PD [30], and ACC [31] are positively correlated with lipid synthesis in adipocytes, exosomal transfer of these enzymes promotes lipid synthesis in recipient cells. In our study, the FASN level in recipient 3T3-L1 preadipocytes was increased after treatment with hypoxic 3T3-L1 adipocyte-derived exosomes. However, the levels of G6PD and ACC were not increased. The reason may be because the high base-line level of G6PD and ACC interrupted the detection of exosome-derived proteins. Moreover, even a slight increase in G6PD has been reported to promote lipogenesis in 3T3-L1 cells [32].

In addition, we found that exosomes purified from ob/ob mice contain detectable FASN, ACC, and G6PD levels compared with those in WT mice. Thus, these exosomal proteins reflect metabolic stress in mammals and may be novel biomarkers, although the origin of exosomes may be non-adipose tissues. Serum FASN is elevated in patients with insulin resistance, although they exosomes have not been examined [33]. Future studies should be conducted to determine how exosomal proteins are incorporated in exosomes and the mechanisms involved.

In conclusion, adipocyte-derived exosomes are potential information carriers under pathological conditions that transfer internal proteins into neighboring cells. Adipocyte-derived exosomes are potential targets for obesity-associated adipose dysfunction.

Conflict of interest and funding

The authors declare no conflict of interest.

Acknowledgments

This study was supported in part by Grant-in-Aid for Scientific Research (24591101) from the Ministry of Education, Science, Sports and Culture, and Hoansha Foundation.

Appendix A. Supplementary data

Supplementary data associated with this article can be found, in the online version, at http://dx.doi.org/10.1016/j.bbrc.2014.01.183.

References

[1] H. van den Bosch, Phosphoglyceride metabolism, Annu. Rev. Biochem. 43 (1974) 243–277.

[2] E.D. Rosen, B.M. Spiegelman, Adipocytes as regulators of energy balance and glucose homeostasis, Nature 444 (2006) 847–853.
[3] A.H. Mokdad, E.S. Ford, B.A. Bowman, W.H. Dietz, F. Vinicor, V.S. Bales, J.S. Marks, Prevalence of obesity, diabetes, and obesity-related health risk factors, 2001, JAMA 289 (2003) 76–79.
[4] L.F. Van Gaal, I.L. Mertens, C.E. De Block, Mechanisms linking obesity with cardiovascular disease, Nature 444 (2006) 875–880.
[5] S.E. Kahn, R.L. Hull, K.M. Utzschneider, Mechanisms linking obesity to insulin resistance and type 2 diabetes, Nature 444 (2006) 840–846.
[6] P. Bjorntorp, Adipose tissue distribution and function, Int. J. Obes. 15 (Suppl. 2) (1991) 67–81.
[7] M. Dunlop, J.M. Court, Lipogenesis in developing human adipose tissue, Early Hum. Dev. 2 (1978) 123–130.
[8] G.P. Laliotis, I. Bizelis, E. Rogdakis, Comparative approach of the de novo fatty acid synthesis (lipogenesis) between ruminant and non ruminant mammalian species: from biochemical level to the main regulatory lipogenic genes, Curr. Genomics 11 (2010) 168–183.
[9] T. Hashimoto, T. Yokokawa, Y. Endo, N. Iwanaka, K. Higashida, S. Taguchi, Modest hypoxia significantly reduces triglyceride content and lipid droplet size in 3T3-L1 adipocytes, Biochem. Biophys. Res. Commun. 440 (2013) 43–49.
[10] S.W. Cushman, L.B. Salans, Determinations of adipose cell size and number in suspensions of isolated rat and human adipose cells, J. Lipid Res. 19 (1978) 269–273.
[11] G. Muller, Let's shift lipid burden – from large to small adipocytes, Eur. J. Pharmacol. 656 (2011) 1–4.
[12] B.T. Pan, R.M. Johnstone, Fate of the transferrin receptor during maturation of sheep reticulocytes in vitro: selective externalization of the receptor, Cell 33 (1983) 967–978.
[13] J.S. Schorey, S. Bhatnagar, Exosome function: from tumor immunology to pathogen biology, Traffic 9 (2008) 871–881.
[14] S. Mathivanan, H. Ji, R.J. Simpson, Exosomes: extracellular organelles important in intercellular communication, J. Proteomics 73 (2010) 1907–1920.
[15] O.G. de Jong, M.C. Verhaar, Y. Chen, P. Vader, H. Gremmels, G. Posthuma, R.M. Schiffelers, M. Gucek, B.W. van Balkom, Cellular stress conditions are reflected in the protein and RNA content of endothelial cell-derived exosomes, J. Extracell Vesicles 1 (2012).
[16] A.S. Azmi, B. Bao, F.H. Sarkar, Exosomes in cancer development, metastasis, and drug resistance: a comprehensive review, Cancer Metastasis Rev. 32 (2013) 623–642.
[17] P. Kucharzewska, H.C. Christianson, J.E. Welch, K.J. Svensson, E. Fredlund, M. Ringner, M. Morgelin, E. Bourseau-Guilmain, J. Bengzon, M. Belting, Exosomes reflect the hypoxic status of glioma cells and mediate hypoxia-dependent activation of vascular cells during tumor development, Proc. Natl. Acad. Sci. U.S.A. 110 (2013) 7312–7317.
[18] H. Tadokoro, T. Umezu, K. Ohyashiki, T. Hirano, J.H. Ohyashiki, Exosomes derived from hypoxic leukemia cells enhance tube formation in endothelial cells, J. Biol. Chem. 288 (2013) 34343–34351.
[19] S. Yu, C. Liu, K. Su, J. Wang, Y. Liu, L. Zhang, C. Li, Y. Cong, R. Kimberly, W.E. Grizzle, C. Falkson, H.G. Zhang, Tumor exosomes inhibit differentiation of bone marrow dendritic cells, J. Immunol. 178 (2007) 6867–6875.
[20] G. Muller, C. Jung, J. Straub, S. Wied, W. Kramer, Induced release of membrane vesicles from rat adipocytes containing glycosylphosphatidylinositol-anchored microdomain and lipid droplet signalling proteins, Cell. Signal. 21 (2009) 324–338.
[21] K. Takahashi, M. Tanaka, A. Inagaki, H. Wanibuchi, Y. Izumi, K. Miura, K. Nagayama, M. Shiota, H. Iwao, Establishment of a 5-fluorouracil-resistant triple-negative breast cancer cell line, Int. J. Oncol. 43 (2013) 1985–1991.
[22] P. Trayhurn, Hypoxia and adipose tissue function and dysfunction in obesity, Physiol. Rev. 93 (2013) 1–21.
[23] M. Eldh, K. Ekstrom, H. Valadi, M. Sjostrand, B. Olsson, M. Jernas, J. Lotvall, Exosomes communicate protective messages during oxidative stress; possible role of exosomal shuttle RNA, PLoS ONE 5 (2010) e15353.
[24] P. Trayhurn, I.S. Wood, Adipokines: inflammation and the pleiotropic role of white adipose tissue, Br. J. Nutr. 92 (2004) 347–355.
[25] B.T. Pan, K. Teng, C. Wu, M. Adam, R.M. Johnstone, Electron microscopic evidence for externalization of the transferrin receptor in vesicular form in sheep reticulocytes, J. Cell Biol. 101 (1985) 942–948.
[26] D. Marimpietri, A. Petretto, L. Raffaghello, A. Pezzolo, C. Gagliani, C. Tacchetti, P. Mauri, G. Melioli, V. Pistoia, Proteome profiling of neuroblastoma-derived exosomes reveal the expression of proteins potentially involved in tumor progression, PLoS ONE 8 (2013) e75054.
[27] K. Strauss, C. Goebel, H. Runz, W. Mobius, S. Weiss, I. Feussner, M. Simons, A. Schneider, Exosome secretion ameliorates lysosomal storage of cholesterol in Niemann-Pick type C disease, J. Biol. Chem. 285 (2010) 26279–26288.
[28] H.W. King, M.Z. Michael, J.M. Gleadle, Hypoxic enhancement of exosome release by breast cancer cells, BMC Cancer 12 (2012) 421.
[29] J.D. Paulauskis, H.S. Sul, Cloning and expression of mouse fatty acid synthase and other specific mRNAs. Developmental and hormonal regulation in 3T3-L1 cells, J. Biol. Chem. 263 (1988) 7049–7054.
[30] J. Park, S.S. Choe, A.H. Choi, K.H. Kim, M.J. Yoon, T. Suganami, Y. Ogawa, J.B. Kim, Increase in glucose-6-phosphate dehydrogenase in adipocytes stimulates oxidative stress and inflammatory signals, Diabetes 55 (2006) 2939–2949.
[31] K.L. Levert, G.L. Waldrop, J.M. Stephens, A biotin analog inhibits acetyl-CoA carboxylase activity and adipogenesis, J. Biol. Chem. 277 (2002) 16347–16350.
[32] J. Park, H.K. Rho, K.H. Kim, S.S. Choe, Y.S. Lee, J.B. Kim, Overexpression of glucose-6-phosphate dehydrogenase is associated with lipid dysregulation and insulin resistance in obesity, Mol. Cell. Biol. 25 (2005) 5146–5157.
[33] J.M. Fernandez-Real, J.A. Menendez, J.M. Moreno-Navarrete, M. Bluher, A. Vazquez-Martin, M.J. Vazquez, F. Ortega, C. Dieguez, G. Fruhbeck, W. Ricart, A. Vidal-Puig, Extracellular fatty acid synthase: a possible surrogate biomarker of insulin resistance, Diabetes 59 (2010) 1506–1511.

Hemodialysis International 2014; **18**:632–640

Enhanced expression of hemoglobin scavenger receptor and heme oxygenase-1 is associated with aortic valve stenosis in patients undergoing hemodialysis

Mayumi INABA,[1] Kenichi SUGIOKA,[2] Takahiko NARUKO,[3] Kei YUNOKI,[3] Yasuyuki KATO,[4] Toshihiko SHIBATA,[4] Takeshi INOUE,[5] Masahiko OHSAWA,[1] Minoru YOSHIYAMA,[2] Makiko UEDA[1]

[1]Department of Pathology, [2]Department of Cardiovascular Medicine, Osaka City University Graduate School of Medicine, Osaka, Japan; [3]Department of Cardiology, [4]Department of Cardiovascular Surgery, [5]Department of Pathology, Osaka City General Hospital, Osaka, Japan

Abstract

A high prevalence and a rapid progression of aortic valve stenosis (AS) in patients undergoing hemodialysis (HD) has been reported. In these circumstances, intraleaflet hemorrhage of aortic valve may be related to the development of AS in HD patients. We immunohistochemically examined the relationship among intraleaflet hemorrhage, neovascularization, hemoglobin scavenger receptor (CD163), and heme oxygenase-1 (HO-1) using surgically resected aortic valve specimens from AS patients undergoing HD. The study population consisted of 26 HD patients and 25 non-HD patients with severe AS who had undergone aortic valve replacement. Frozen aortic valve samples surgically obtained from AS patients were stained immunohistochemically with antibodies against smooth muscle cells, macrophages, glycophorin-A (a protein specific to erythrocyte membranes), CD31, CD163, and HO-1. Morphometric analysis demonstrated that the CD163-positive macrophage score, the number of CD31-positive microvessels, and the percentage of glycophorin-A and HO-1-positive area were significantly higher in HD patients than in non-HD patients (CD163-positive macrophage score, $P < 0.0001$; CD31-positive microvessels, $P < 0.0001$; glycophorin-A, $P < 0.0001$; HO-1, $P < 0.0001$). Double immunostaining for CD163 or HO-1 and macrophages revealed that the majority of CD163- or HO-1-positive cells were macrophages. Furthermore, CD163-positive macrophage score was positively correlated with glycophorin-A, HO-1-positive area, and the number of CD31-positive microvessels (glycophorin-A, $R = 0.66$, $P < 0.0001$; HO-1, $R = 0.50$, $P < 0.0005$; microvessels, $R = 0.38$, $P < 0.01$). These findings suggest a positive association among intraleaflet hemorrhage, neovascularization, and enhanced expression of CD163 and HO-1 as a response to intraleaflet hemorrhage in stenotic aortic valves in AS patients undergoing HD.

Key words: Aortic valve stenosis, hemodialysis, intraleaflet hemorrhage, CD163, HO-1

Correspondence to: M. Ueda, MD, Department of Pathology, Osaka City University Graduate School of Medicine, 1-4-3 Asahi-machi, Abeno-ku, Osaka 545-8585, Japan. E-mail: maki@med.osaka-cu.ac.jp

Conflict of interest statement: None declared.

INTRODUCTION

Patients undergoing hemodialysis (HD) have a greater prevalence of aortic valve calcification and aortic valve stenosis (AS).[1,2] Furthermore, AS progresses more rapidly in HD patients than in non-HD patients.[3,4] However, the

DOI:10.1111/hdi.12147

precise mechanism of the relationship between HD treatment and rapid development of AS is still unknown. Previously, Kajbaf et al.[5] showed that surgically removed aortic valves in AS patients with HD had a significant increase in inflammatory cells and neovascularization, indicating that development of AS in HD patients is a more aggressive process in aortic valve leaflet with inflammation and neoangiogenesis than that in non-HD patients. Very recently, we reported that plasma levels of oxidized low-density lipoprotein (ox-LDL) and myeloperoxidase (MPO), a neutrophil-derived enzyme that catalyzes the formation of reactive oxidant species, significantly increased after a single HD session, and that there was a direct association between plasma MPO levels and plasma ox-LDL levels during initial HD.[6] Therefore, patients undergoing HD are under the severe levels of oxidative stress that could contribute to cellular damage, leading to inflammation and neoangiogenesis in aortic valves.

Recent studies have revealed that intraplaque hemorrhage is associated with the progression of atherosclerotic lesions and plaque instability.[7–10] In coronary atherosclerotic plaques, we have shown a close association among oxidative stress, neovascularization, and intraplaque hemorrhage.[11] Immune activation in response to intraplaque hemorrhages is reflected by the induction of CD163 and heme oxygenase-1 (HO-1). CD163 is recognized as the specific macrophage receptor for hemoglobin-haptoglobin (Hb-Hp) complexes, responsible for the clearance of Hb,[12,13] and binding of Hb to CD163 induces HO-1, which is a cytoprotective enzyme that is induced by intraplaque hemorrhage and degrades free heme and releases ferrous iron, which is rapidly sequestered by ferritin.[14,15] Induction of HO-1 via CD163-Hb transport is an important step in the Hb clearance pathway in the macrophage, especially under condition of intraplaque hemorrhage leading to extreme Hb release.[16] We have previously demonstrated that CD163 is overexpressed in accumulated macrophages of coronary atherosclerotic lesions in patients with unstable angina pectoris.[11]

A recent study showed that intraleaflet hemorrhage in aortic valve was associated with 4-hydroxy-2 nonenal, a major product of lipid peroxidation, neovascularization, and rapid progression of AS in non-HD patients.[17] We hypothesize that intraleaflet hemorrhage is also closely associated with a rapid development of AS in HD patients and that CD163 and HO-1 play a critical role in AS progression in patients undergoing HD; however, the localization and relationship of hemorrhage in aortic valve, neovascularization, and the expression of CD163 and HO-1 have not been evaluated in HD patients. Therefore, we investigated the immunolocalization and association of intraleaflet hemorrhage, neovascularization, and the expression of CD 163 and HO-1 using surgically resected aortic valve specimens from AS patients undergoing HD.

METHOD

Study population

Aortic valve specimens were obtained in 108 consecutive patients undergoing aortic valve replacement (AVR) for degenerative AS at Osaka City General Hospital between May 2008 and April 2012. Patients with infectious endocarditis (n = 13), rheumatic valvular heart disease (n = 5), congenital abnormality of valves (n = 5), and chronic inflammatory disease (n = 7) such as collagen disease and malignancy were excluded. We also excluded patients for which frozen aortic valve specimens were not available (n = 27). Ultimately, 51 patients were enrolled in the study. Of these 51 patients, 26 had chronic renal failure on HD and 25 were non-HD patients. Immediately after AVR, the tissue specimens were snap frozen, and stored at −80°C. In addition, frozen aortic valve specimens obtained at autopsy from individuals who died of noncardiovascular causes (n = 11) were used as references (mean age 68). The snap-frozen samples obtained by AVR were serially sectioned to produce sections of 5 μm in thickness, and then fixed in acetone. The first section of each sample was stained with hematoxylin–eosin stain. Subsequent sections were used for immunohistochemical staining.

To define the presence of chronic kidney disease (CKD), we applied the Modification of Diet in Renal Disease Study equation for evaluating Japanese CKD patients:[18,19] $0.741 \times 175 \times \text{age}^{0.203} \times (\text{serum creatinine})^{1.154} \times (0.742$ for female) mL/min/1.73 m^2. Chronic kidney disease was defined as estimated glomerular filtration rate (eGFR) <60 mL/min/1.73 m^2. The degree of renal dysfunction was graded as follows: CKD stage 1: minimal damage to kidneys with normal renal function, eGFR ≥90 mL/min/1.73 m^2; CKD stage 2: mild renal dysfunction, 60 ≤ eGFR <90 mL/min/1.73 m^2; CKD stage 3: moderate renal dysfunction, 30 ≤ eGFR <60 mL/min/1.73 m^2; CKD stage 4: severe renal dysfunction, 15 ≤ eGFR <30 mL/min/1.73 m^2; CKD stage 5: end-stage renal dysfunction, eGFR <15 mL/min/1.73 m^2 or HD. In 25 non-HD patients, there were eight patients with CKD (seven patients with CKD stage 3 and one patient with CKD stage 4).

Clinical data were obtained from medical charts. Hypertension, hyperlipidemia, and diabetes mellitus criteria followed the guideline of each society. All patients underwent preoperative echocardiography by experienced sonographers. The severity of AS and cardiac function was assessed by using transthoracic echocardiography. The continuity equation was utilized to calculate aortic valve area. Left ventricular end-diastolic volume, end-systolic volume, and ejection fraction were also calculated. The study was approved by the hospital's ethics committee, and informed consent was obtained from all patients before the study.

Immunohistochemistry

Single immunostaining

The sources and specificity of all antibodies used in this study are summarized in the supplementary file. Microvessels of the tissue sections were assessed using antibodies for CD31 (DAKO, Glostrup, Denmark), CD34 (DAKO), and von Willebrand factor (DAKO). MPO (MPO-7, DAKO) was used as pro-oxidant enzyme. Sections were incubated at 4°C overnight or for 1 hour at room temperature, and then a three-step indirect streptavidin-biotin technique with peroxidase was used, followed by final visualization of the peroxidase activity with 3-amino-9- ethylcarbazole used as chromogen. Nuclei were faintly counterstained with hematoxylin. In negative controls, the primary antibody was replaced by an irrelevant mouse monoclonal antibody of the same subclass.

Double immunostaining

To identify CD163- or HO-1-positive cells, we performed double immunostaining for macrophages (CD68) and CD163 or HO-1 using modifications of procedures reported previously.[20] For double immunostaining, alkaline phosphatase was visualized with fast blue BB (blue: CD68) and peroxidase with 3-amino-9-ethylcarbazole development (red: CD163 or HO-1). In addition, simultaneous identification of smooth muscle cells and macrophages was performed using two primary antibodies to different IgG subclass proteins (1A4/CD68), as reported previously.[20] The enzymatic activity of β-galactosidase for 1A4 was presented as turquoise (BioGenex Kit, BioGenex, CA, USA), while alkaline phosphatase for CD68 was presented as red (New Fuchsin Kit, DAKO).

Quantitative methods

We have used the Win Roof ver. 6.40 (Mitani Corporation, Tokyo, Japan) for the quantitative method for immunostaining. The tissue area occupied by immunostained macrophages or glycophorin-A-, CD163-, HO-1-, IL-10-, and ferritin-positive areas was quantified using computer-aided planimetry and expressed as a percentage of the total surface area of the tissue section. Based on these quantifications, a "CD163-positive macrophage score" was calculated as the ratio of the CD163-positive area to the macrophage-positive area. Microvessels were investigated based on the analysis of CD31-, CD34-, and von Willebrand factor-positive endothelial cells forming tubular structures. In this study, the number of CD31-positive endothelial cells forming tubular structures was counted in the entire tissue section, and expressed as the number of microvessels per mm^2 of the tissue. The morphometric analysis was performed by a single investigator who was blinded to the patients' characteristics and histological classifications.

Statistical analysis

The results are expressed as a mean ± SD and as a percentage for categorical variables. For continuous variables, the two groups of patients (HD and non-HD) were compared with a Mann-Whitney U test. When comparing three groups of individuals, the nonparametric Kruskal-Wallis test was used. We compared categorical variables using a chi-square test or Fisher's exact test. Values of $P < 0.05$ were considered significant.

RESULTS

Patients' characteristics

Patients' demographics and echocardiographic data are shown in Table 1. There were no differences with respect to age, presence of hypertension, smoking, and prevalence of angiotensin-converting enzyme/angiotensin II receptor blocker treatment between HD and non-HD patients. However, prevalence of male and coronary artery disease was significantly higher, and prevalence of diabetes mellitus, hypercholesterolemia and statin treatment, and body mass index were lower in HD patients than in non-HD patients. Echocardiographic data showed no differences in aortic valve area and left ventricular ejection fraction.

Histological findings

In the lesions of HD patients, there were abundant macrophages, large numbers of microvessels, and MPO-positive cells (Figure 1A2–A4). In these lesions, erythrocytes were present (Figure 1A5). In addition, the

Table 1 Patients' characteristics

	HD (n = 26)	Non-HD (n = 25)	P value
Age, years	72 ± 7	76 ± 7	0.06
Male (%)	17 (65)	8 (32)	0.01
Body mass index (kg/m^2)	20 ± 3	24 ± 4	<0.0001
Hypertension (%)	19 (73)	23 (92)	0.07
Hypercholesterolemia (%)	7 (27)	14 (56)	0.02
Diabetes mellitus (%)	5 (19)	11 (44)	0.047
Smoking (%)	5 (21)	2 (10)	0.50
Coronary artery disease (%)	19 (73)	3 (12)	0.003
ACEI/ARB (%)	10 (38)	13 (52)	0.21
Statins (%)	4 (15)	8 (32)	0.02
Aortic valve area (cm^2)	0.72 ± 0.16	0.76 ± 0.28	0.40
LVEF (%)	55 ± 13	65 ± 10	0.08

ACEI = angiotensin-converting enzyme inhibitor; ARB = angiotensin II receptor blocker; HD = hemodialysis; LVEF = left ventricular ejection fraction.

sites with abundant CD163-positive macrophages approximately colocalized with the site of erythrocytes (Figure 1A6). HO-1 positive cells were also found in these lesions (Figure 1A7). In contrast, scattered macrophages were seen in the lesions of non-HD patients (Figure 1B2). Endothelial cells were present at the surface area, but microvessels were not seen (Figure 1B3). In these lesions, there were no erythrocytes (Figure 1B5). The anti-CD163 antibody indicated that the scattered macrophages were negative for CD163- and HO-1-positive cells (Figure 1B6,B7). In the lesions of HD patients, double immunostaining for CD163 or HO-1 and macrophages revealed that the majority of CD163- or HO-1-positive cells were macrophages (Figure 2A1–A3). In the aortic valve specimens from reference cases, there were scattered macrophages, but no microvessels, erythrocytes, and CD163- or HO-1-positive cells were found (Figure 1C1–C8).

Morphometric analysis

Morphometric results are shown in Figure 3. Quantitative analysis demonstrated that the percentage of the macrophage-positive area was significantly higher among HD patients than among either non-HD patients or reference cases (HD vs. non-HD, $P < 0.01$; HD vs. reference, $P < 0.0001$). In addition, the number of CD31-positive microvessels was significantly higher in HD patients than in either non-HD patients or reference cases (HD vs. non-HD, $P < 0.001$; HD vs. reference, $P < 0.0001$). Compared with lesions from non-HD patients or reference cases, lesions from HD patients had significantly higher glycophorin-A-positive areas (HD vs. non-HD, $P < 0.0001$; HD vs. reference, $P < 0.0001$). The CD163-positive macrophage score was also significantly higher in HD patients than in non-HD patients or reference cases (HD vs. non-HD, $P < 0.0001$; HD vs. reference, $P < 0.0001$). Furthermore, the percentage of the HO-1-positive area was significantly higher in HD patients than in either non-HD patients or reference cases (HD vs. non-HD, $P < 0.0001$; HD vs. reference, $P < 0.0001$). The CD163-positive macrophage score positively correlated with the glycophorin- A-positive area, the HO-1-positive area, and the number of CD31-positive microvessels (CD163 vs. glycophorin-A, $R = 0.66$, $P < 0.0001$; CD163 vs. HO-1, $R = 0.50$, $P < 0.0005$; CD163 vs. microvessels, $R = 0.38$, $P < 0.01$). Moreover, the number of CD31-positive microvessels positively correlated with the number of MPO-positive cells ($R = 0.73$, $P < 0.0001$).

We evaluated the differences observed in the study parameters between CKD and non-CKD in non-HD patients. In the present study, however, we did not find any differences in the macrophage-positive area, the number of CD31-positive microvessels, the glycophorin-A-positive area, the CD163-positive macrophage score, and the HO-1-positive area between the two groups.

DISCUSSION

To the best of our knowledge, this study is the first to report that expressions of Hb scavenger receptor CD163 and HO-1 were enhanced in aortic valve in AS patients undergoing HD by analyzing frozen sections of surgically resected aortic valve specimens. Furthermore, we also demonstrated a positive association among neovascularization, intraleaflet hemorrhage, and the expression

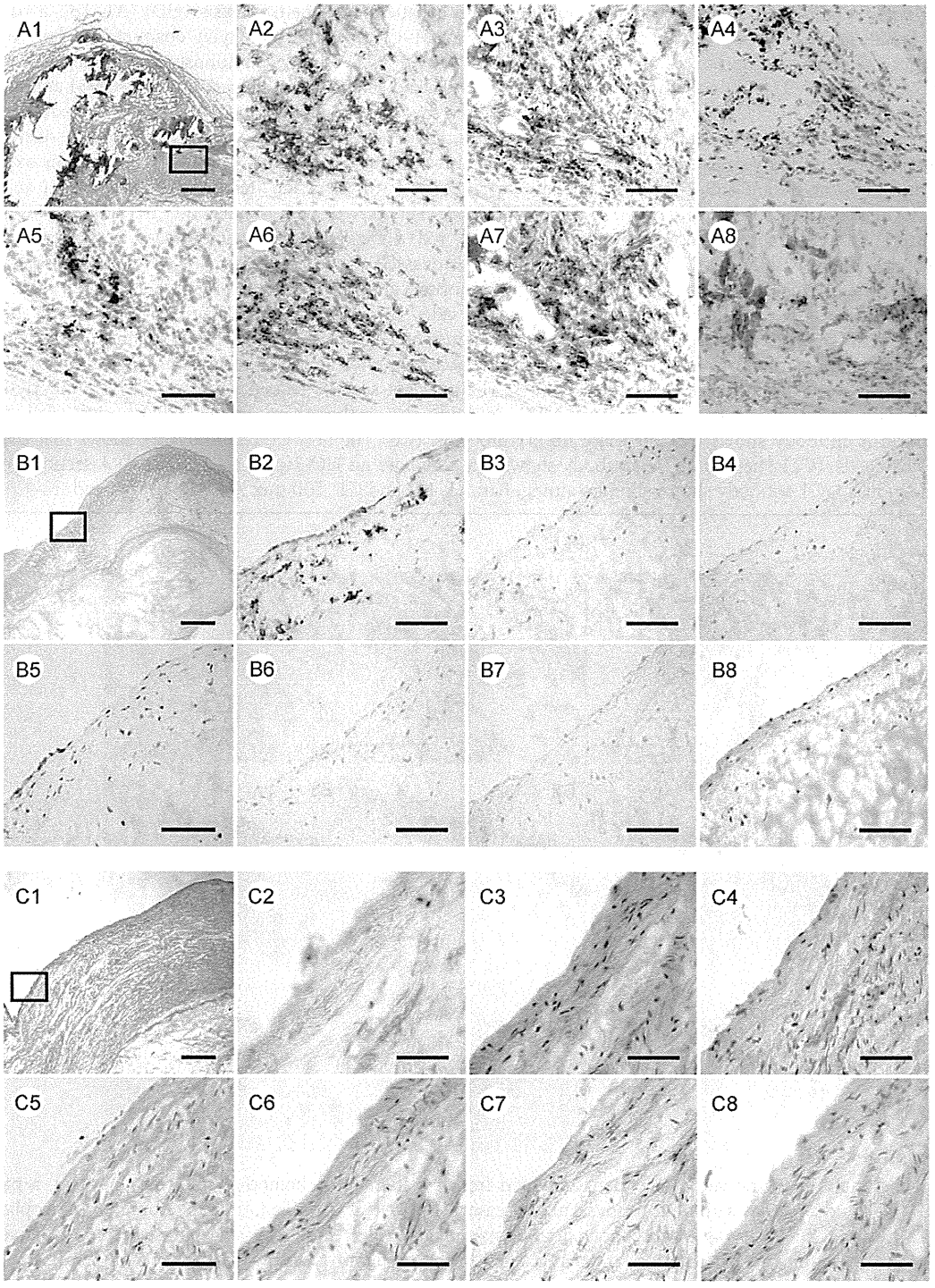
A1
A2
A3
A4
A5
A6
A7
A8
B1
B2
B3
B4
B5
B6
B7
B8
C1
C2
C3
C4
C5
C6
C7
C8

Figure 1 Micrographs of aortic valve specimens obtained from a patient with hemodialysis (HD) (A1–A8), a patient with non-HD (B1–B8), and a patient with noncardiovascular disease (C1–C8). (A1) Hematoxylin–eosin stain. The cross section shows distinct calcification. The boxed area is enlarged in (A2)–(A8). (A2) Double immunostaining (smooth muscle cells, turquoise; macrophage, red) reveals abundant macrophages. (A3) The adjacent section stained with anti-CD31 antibody reveals a large number of CD31-positive microvessels. (A4) The adjacent section stained with anti-MPO (myeloperoxidase) antibody reveals that abundant MPO-positive cells are present. (A5) The antiglycophorin-A antibody shows the presence of erythrocytes. (A6) The anti-CD163 antibody shows that abundant CD163-positive cells are present. (A7) The anti-HO-1 (heme oxygenase-1) antibody shows that abundant HO-1-positive cells are also present. (A8) A section treated with nonimmune mouse IgG1 antibody shows absent staining. (B1) Hematoxylin–eosin stain. The boxed area is enlarged in (B2)–(B8). (B2) Double immunostaining (smooth muscle cells, turquoise; macrophage, red) shows scattered macrophages in the lesion. (B3) The adjacent section stained with anti-CD31 antibody reveals no microvessels with CD31 positivity. (B4) The anti-MPO antibody shows that there are no MPO-positive cells. (B5) The antiglycophorin-A antibody shows that there are no erythrocytes. (B6) The anti-CD163 antibody shows that there are no CD163-positive cells. (B7) The anti-HO-1 antibody shows that there are no HO-1-positive cells. (B8) A section treated with nonimmune mouse IgG1 antibody shows absent staining. (C1) Hematoxylin–eosin stain. The boxed area is enlarged in (C2)–(C8). (C2) Double immunostaining (smooth muscle cells, turquoise; macrophage, red) shows a few macrophages in the lesion. (C3) The adjacent section stained with anti-CD31 antibody reveals no microvessels with CD31 positivity. (C4) The anti-MPO antibody shows that there are no MPO-positive cells. (C5) The antiglycophorin-A antibody shows that there are no erythrocytes. (C6) The anti-CD163 antibody shows that there are no CD163-positive cells. (C7) The anti-HO-1 antibody shows that there are no HO-1-positive cells. (C8) A section treated with nonimmune mouse IgG1 antibody shows absent staining. Bar: A1, B1, and C1: 500 μm; A2–A8, B2–B8, and C2–C8: 100 μm.

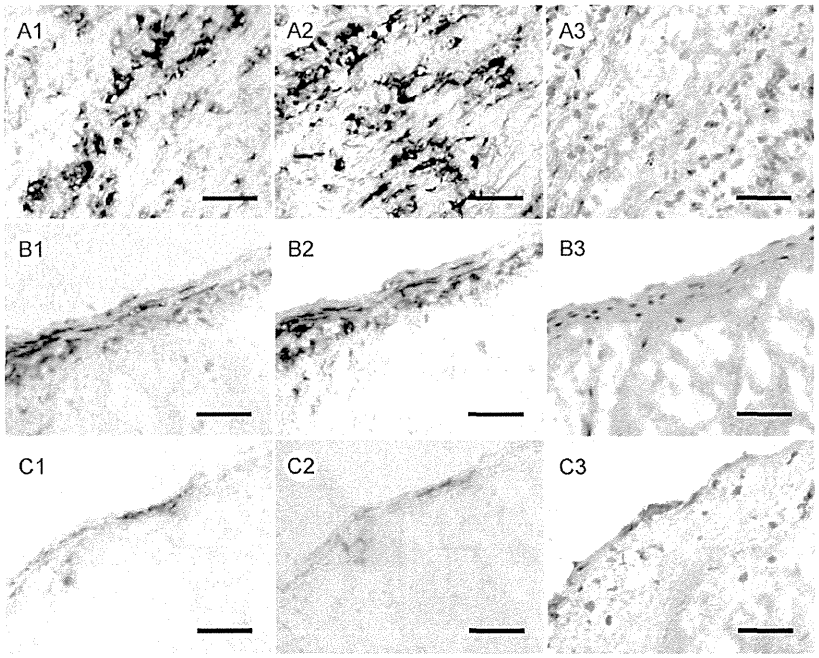

Figure 2 Micrographs of aortic valve specimens obtained from a patient with hemodialysis (HD) (A1–A3), a patient with non-HD (B1–B3), and a patient with noncardiovascular disease (C1-C3). (A1) Double immunostaining for macrophages (blue) and CD163 (red) reveals that most cells show double staining (purple), indicating that most CD163-positive cells are macrophages. (A2) Double immunostaining for macrophages (blue) and heme oxygenase-1 (HO-1) (red) reveals that most cells show double staining (purple), indicating that the vast majority of HO-1-positive cells are macrophages. (A3) Absent staining after use of nonimmune mouse IgG1 antibodies. (B1, C1) Double immunostaining for macrophages (blue) and CD163 (red) reveals that there are no CD163-positive macrophages. (B2, C2) Double immunostaining for macrophages (blue) and HO-1 (red) reveals that there are no HO-1-positive macrophages. (B3, C3) Absent staining after use of nonimmune mouse IgG1 antibodies. Bar: 50 μm.

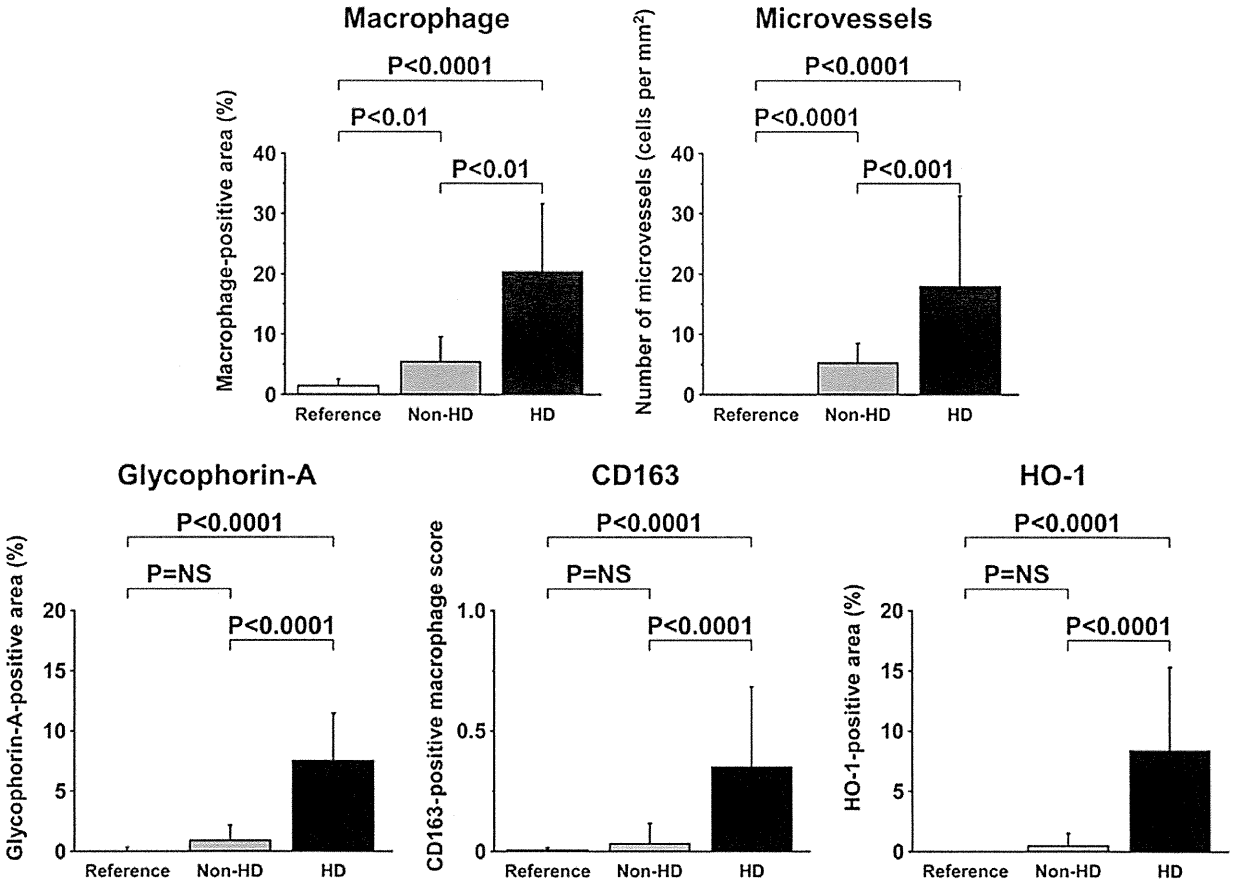

Figure 3 Graphs showing the macrophage-, glycophorin-A-, and HO-1-positive areas expressed as a percentage of the total surface area, the number of microvessels per mm^2, and the CD163-positive macrophage score in the aortic valve specimens obtained from reference cases, non-HD (hemodialysis) patients, and HD patients. HO-1 = heme oxygenase-1.

of CD163 and HO-1. These observations suggest that enhanced expression of CD163 and HO-1 as a response to intraleaflet hemorrhage may exert anti-inflammatory effects in stenotic aortic valves in AS patients undergoing HD.

Aortic valve calcification has been shown to present an active cellular-mediated process associated with inflammation,[21–23] oxidative stress,[24,25] and neoangiogenesis.[26,27] Moreover, a recent study reported that intraleaflet hemorrhage of aortic valve was frequently observed in AS patients with rapid progression, indicating that occurrence of intraleaflet hemorrhage in aortic valve may also be an important factor for the rapid progression of AS.[17] In the present study, the number of CD31-positive microvessels and the percentage of glycophorin-A were significantly higher in HD patients than in non-HD patients, and there was a positive correlation between CD31-positive microvessels and glycophorin-A. These findings support the hypothesis of a close relationship between neovascularization and intraleaflet hemorrhage in HD patients.

HD treatment causes an increase in neutrophil activation and enhanced oxidative stress. Accordingly, circulating levels of MPO and ox-LDL increase during the maintenance of HD.[6,28,29] Ox-LDL induces a dramatic cytotoxic effect on endothelial cells, and also upregulates the expression of vascular endothelial growth factor, one of the angiogenesis-promoting factors, in injured endothelial cells and accumulated macrophages.[30] In the present study, we demonstrated that the number of microvessels positively correlated with the number of MPO-positive cells in HD patients. These data support the concept that biomarkers regarding oxidative stress due to HD treatment could induce not only tissue damages but also neovascularization and, subsequently, extravasation of

red blood cells from leaky microvessels in the aortic valves.

The present study demonstrated that a higher expression of CD163 and HO-1 was found in aortic valve lesions in HD patients than in non-HD patients, and the number of CD163- and HO-1-positive macrophage scores was positively correlated with intraleaflet hemorrhage and the number of neovascularization. These observations indicate that intraleaflet hemorrhage from leaky microvessels may induce HO-1 via CD163-Hb transport, and that enhanced expression of CD163 and HO-1 is a critical process which could occur as a response to intraleaflet hemorrhage induced by oxidative stress during HD treatment. Effective clearance of extracellular Hb is thought to limit systemic oxidative heme toxicity.[31,32] Cell-free Hb is tightly bound to Hp and subsequently cleared by CD163.[12] Binding of Hb to CD163 induces HO-1. HO-1 catalyzes the regiospecific oxidative degradation of free heme into ferrous iron, which is rapidly sequestered by ferritin, one of the antioxidative and anti-inflammatory end products linked to heme breakdown.[14,15] Therefore, induction of HO-1 is directly involved in the downregulation of inflammation and oxidative stress, and contributes to improvement of the balance of inflammation and oxidative stress.

There are several limitations in our study. First, the study population is relatively small. Furthermore, the homogeneity of the two study groups is poor that differ for incidence of diabetes, sex, and cardiovascular risk factors such as hypercholesterolemia. Second, early lesions of aortic valve sclerosis in patients undergoing HD were not included in the present study. However, it is extremely difficult to obtain frozen samples of such early lesions during surgery. Third, the partial difference in distribution of intraleaflet hemorrhage, CD163, and HO-1 was observed in the lesions of AS in HD patients. The difference in distribution observed in our study may provide the difference of time phase of expression in the cascade of Hb-CD163-mediated HO-1 pathway. Finally, the measurement of levels of soluble CD163 is important to understand the relationship between CD163 and AS in HD patients. However, soluble CD163 data are not available in the present study. Future study should evaluate the levels of soluble CD163 in AS patients undergoing HD.

In conclusion, the present study revealed the associations among extravasation of red blood cells from leaky microvessels leading to intraleaflet hemorrhage, enhanced expression of Hb scavenger receptor CD163, and HO-1 in human stenotic aortic valve leaflet undergoing HD. These findings suggest a pivotal process for enhanced expression of CD163 and HO-1 which could occur as a response to intraleaflet hemorrhage, and could contribute to improvement of the balance of inflammation and oxidative stress during the progression of AS in HD patients.

Manuscript received June 2013; revised December 2013.

REFERENCES

1 Maher ER, Young G, Smyth-Walsh B, Pugh S, Curtis JR. Aortic and mitral valve calcification in patients with end-stage renal disease. *Lancet*. 1987; **2**:875–877.

2 Straumann E, Meyer B, Misteli M, Blumberg A, Jenzer HR. Aortic and mitral valve disease in patients with end stage renal failure on long-term hemodialysis. *Br Heart J*. 1992; **67**:236–239.

3 Perkovic V, Hunt D, Griffin SV, du Plessis M, Becker GJ. Accelerated progression of calcific aortic stenosis in dialysis patients. *Nephron Clin Pract*. 2003; **94**:c40–c45.

4 Ohara T, Hashimoto Y, Matsumura A, Suzuki M, Isobe M. Accelerated progression and morbidity in patients with aortic stenosis on chronic dialysis. *Circ J*. 2005; **69**:1535–1539.

5 Kajbaf S, Veinot JP, Ha A, Zimmerman D. Comparison of surgically removed cardiac valves of patients with ESRD with those of the general population. *Am J Kidney Dis*. 2005; **46**:86–93.

6 Kitabayashi C, Naruko T, Sugioka K, et al. Positive association between plasma levels of oxidized low density lipoprotein and myeloperoxidase after hemodialysis in patients with diabetic end-stage renal disease. *Hemodialysis Int*. 2013; **17**:557–567.

7 Kolodgie FD, Gold HK, Burke AP, et al. Intraplaque hemorrhage and progression of coronary atheroma. *N Engl J Med*. 2003; **349**:2316–2325.

8 Moreno PR, Purushothaman KR, Fuster V, et al. Plaque neovascularization is increased in ruptured atherosclerotic lesions of human aorta: Implications for plaque vulnerability. *Circulation*. 2004; **110**:2032–2038.

9 Virmani R, Kolodgie FD, Burke AP, et al. Atherosclerotic plaque progression and vulnerability to rupture: Angiogenesis as a source of intraplaque hemorrhage. *Arterioscler Thromb Vasc Biol*. 2005; **25**:2054–2061.

10 Pelisek J, Well G, Reeps C, et al. Neovascularization and angiogenic factors in advanced human carotid artery stenosis. *Circ J*. 2012; **76**:1274–1282.

11 Yunoki K, Naruko T, Komatsu R, et al. Enhanced expression of haemoglobin scavenger receptor in accumulated macrophages of culprit lesions in acute coronary syndromes. *Eur Heart J*. 2009; **30**:1844–1852.

12 Kristiansen M, Graversen JH, Jacobsen C, et al. Identification of the haemoglobin scavenger receptor. *Nature*. 2001; **409**:198–201.

13 Graversen JH, Madsen M, Moestrup SK. CD163: A signal receptor scavenging haptoglobin-hemoglobin complexes from plasma. *Int J Biochem Cell Biol.* 2002; **34**:309–314.
14 Philippidis P, Mason JC, Evans BJ, et al. Hemoglobin scavenger receptor CD163 mediates interleukin-10 release and heme oxygenase-1 synthesis: Anti-inflammatory monocyte-macrophage responses in vitro, in resolving skin blisters in vivo, and after cardiopulmonary bypass surgery. *Circ Res.* 2004; **94**:119–126.
15 Schaer CA, Schoedon G, Imhof A, Kurrer MO, Schaer DJ. Constitutive endocytosis of CD163 mediates hemoglobin-heme uptake and determines the noninflammatory and protective transcriptional response of macrophages to hemoglobin. *Circ Res.* 2006; **99**:943–950.
16 Abraham NG, Drummond G. CD163-mediated hemoglobin-heme uptake activates macrophage HO-1, providing an antiinflammatory function. *Circ Res.* 2006; **99**:911–914.
17 Akahori H, Tsujino T, Naito Y, et al. Intraleaflet haemorrhage is associated with rapid progression of degenerative aortic valve stenosis. *Eur Heart J.* 2011; **32**:888–896.
18 Levey AS, Coresh J, Greene T, et al. Using standardized serum creatinine values in the Modification of Diet in Renal Disease Study equation for estimating glomerular filtration rate. *Ann Intern Med.* 2006; **145**:247–254.
19 Imai E, Horio M, Nitta K, et al. Modification of the Modified Diet Renal Disease (MDRD) study equation for Japan. *Am J Kidney Dis.* 2007; **50**:927–937.
20 van der Loos CM, Becker AE, van den Oord JJ. Practical suggestions for successful immunoenzyme double-staining experiments. *Histochem J.* 1993; **25**:1–13.
21 Otto CM, Kuusisto J, Reichenbach DD, Gown AM, O'Brien KD. Characterization of the early lesion in "degenerative" valvular aortic stenosis: Histological and immunohistochemical studies. *Circulation.* 1994; **90**:844–853.
22 Olsson M, Dalsgaard CJ, Haegerstrand A, Rosenqvist M, Rydén L, Nilsson J. Accumulation of T lymphocytes and expression of interleukin-2 receptors in nonrhumatic stenotic aortic valves. *J Am Coll Cardiol.* 1994; **23**:1162–1170.
23 Mohler ER 3rd, Gannon F, Reynolds C, Zimmerman R, Keane MG, Kaplan FS. Bone formation and inflammation in cardiac valves. *Circulation.* 2001; **103**:1522–1528.
24 Liberman M, Bassi E, Martinatti MK, et al. Oxidant generation predominates around calcifying foci and enhances progression of aortic valve calcification. *Arterioscler Thromb Vasc Biol.* 2008; **28**:463–470.
25 Miller JD, Chu Y, Brooks RM, Richenbacher WE, Peña-Silva R, Heistad DD. Dysregulation of antioxidant mechanisms contributes to increased oxidative stress in calcific aortic valvular stenosis in humans. *J Am Coll Cardiol.* 2008; **52**:843–850.
26 Soni Y, Salo T, Satta J. Angiogenesis is involved in the pathogenesis of nonrheumatic aortic valve stenosis. *Hum Pathol.* 2003; **34**:756–763.
27 Mazzone A, Epistolato MC, De Caterina R, et al. Neoangiogenesis, T-lymphocyte infiltration, and heat shock protein-60 are biological hallmarks of an immunomediated inflammatory process in end-stage calcified aortic valve stenosis. *J Am Coll Cardiol.* 2004; **43**:1670–1676.
28 Rutgers A, Heeringa P, Kooman JP, van der Sande FM, Cohen Travaert JW. Peripheral blood myeloperoxidase activity increases during hemodialysis. *Kidney Int.* 2003; **64**:760.
29 Borawski J. Myeloperoxidase as a marker of hemodialysis biocompatibility and oxidative stress: The underestimated modifying effects of heparin. *Am J Kidney Dis.* 2006; **47**:37–41.
30 Inoue M, Itoh H, Tanaka T, et al. Oxidized LDL regulates vascular endothelial growth factor expression in human macrophages and endothelial cells through activation of peroxisome proliferator-activated receptor-γ. *Arterioscler Thromb Vasc Biol.* 2001; **21**:560–566.
31 Jeney V, Balla J, Yachie A, et al. Pro-oxidant and cytotoxic effects of circulating heme. *Blood.* 2002; **100**:879–887.
32 Rother RP, Bell L, Hillmen P, Gladwin MT. The clinical sequelae of intravascular hemolysis and extracellular plasma hemoglobin: A novel mechanism of human disease. *JAMA.* 2005; **293**:1653–1662.

SUPPORTING INFORMATION

Additional Supporting Information may be found in the online version of this article at the publisher's web-site:

Table S1 Antibody used in the study.

European Heart Journal - Cardiovascular Imaging Advance Access published June 17, 2014

IMAGE FOCUS

doi:10.1093/ehjci/jeu119

Chronic active Epstein–Barr virus infection complicated with multiple artery aneurysms

Satoshi Nishimura*, Shoichi Ehara, Akihisa Hanatani, and Minoru Yoshiyama

Department of Cardiovascular Medicine, Osaka City University Graduate School of Medicine, 1-4-3 Asahi-machi, Abeno-ku, Osaka 545-8585, Japan

* Corresponding author. Tel: +81 6 66453801; Fax: +81 6 66466808. E-mail: satoshirx8@yahoo.co.jp, a96m050@med.osaka-cu.ac.jp

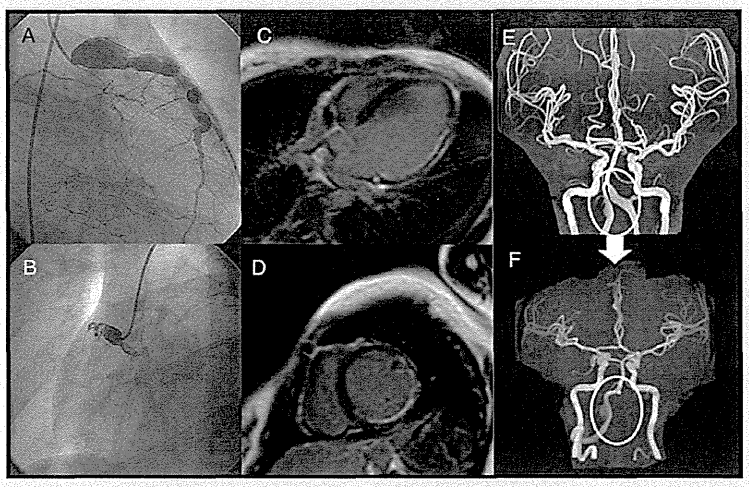

A 26-year-old woman was admitted to our hospital to undergo allogeneic peripheral blood stem cell transplantation for the treatment of chronic active Epstein–Barr virus (CAEBV) infection.

Transthoracic echocardiography showed hypokinetic inferior, posterior, and lateral left ventricular (LV) walls. Coronary angiography demonstrated large aneurysms in the proximal left (LCA) and right coronary arteries (RCA). The LCA aneurysm was located in the bifurcation of the left anterior descending (LAD) and left circumflex arteries (LCx), and the LCx was occluded at the diverging point from the left main coronary artery. The RCA was occluded by the distal portion of the aneurysm. Distal vessels to the occlusion sites of the LCx and RCA presented collateral vessels from the LAD (*Panels A* and *B*). Late gadolinium enhancement on cardiac magnetic resonance (MR) imaging revealed subendocardial enhancement within the LV walls, which corresponded with the occluded LCx and RCA territories (*Panels C* and *D*). Further screening was performed with MR angiography, which showed bilateral vertebral artery aneurysms (*Panel E*). Five months later, asymptomatic occlusion was also found in the left vertebral artery (*Panel F*).

Rarely, the primary infection of Epstein–Barr virus in T or natural killer cells induces CAEBV infection, a fatal syndrome characterized by infectious mononucleosis-like chronic symptoms that affect both children and young adults. Patients with CAEBV often develop multiple artery aneurysms, which are clinically silent until they rupture or cause organ damage. Therefore, screening for cardiovascular complications is indispensable in patients with CAEBV.